Grafted polymer monolayer brush as electron beam resist

by

Hirotaka Yamada

A thesis
presented to the University of Waterloo
in fulfillment of the
thesis requirement for the degree of
Master of Applied Science
in
Electrical and Computer Engineering (Nanotechnology)

Waterloo, Ontario, Canada, 2017

© Hirotaka Yamada 2017

AUTHOR'S DECLARATION

I hereby declare that I am the sole author of this thesis. This is a true copy of the thesis, including any required final revisions, as accepted by my examiners.

I understand that my thesis may be made electronically available to the public.

Abstract

This thesis focuses on the nanofabrication process using novel electron beam resists. First, in Chapter 3 and Chapter 4, the nanofabrication process using grafted polymer monolayer brush as e-beam resist was examined. Then, in Chapter 5, characteristics of the mixture of polystyrene (PS) and polydimethylsiloxane (PDMS) as negative tone e-beam resist with high dry etch resistance were studied.

The main advantage of grafted polymer brush as electron beam is that it is applicable on non-flat or irregular surfaces. Although nanofabrication on non-flat surfaces has a lot of applications such as nanofabrication on AFM tips and optical fibers, there is no versatile method for nanofabrication on non-flat surfaces. In this thesis, nanofabrication on non-flat surfaces of an AFM cantilever was demonstrated using grafted polymer brush. Grafted polymer brush includes grafted poly(methyl methacrylate) (PMMA) brush and grafted PS brush; PMMA brush was used as negative tone e-beam resist, and PS monolayer brush was used as both positive and negative tone e-beam resist in this study.

When PMMA brush and PS brush are used as negative tone resist, a development method plays an important role. Although solvent development is the most common development method to develop thick PMMA film or PS film as negative tone resist, solvent does not work as a developer for PMMA brush and PS brush. Instead, thermal treatment was used to develop monolayer PMMA brush or PS brush to achieve negative tone behavior. Since cross-linked PMMA and PS has higher thermal stability than uncross-linked ones, only unexposed polymer was vaporized at proper temperature. Thus, the polymer brush works as negative tone resist.

Positive tone behavior of PS brush was achieved by changing the development method. When PS is exposed to electron beam, it loses the resistance to wet etch. Therefore, when the PS

brush was grafted on an intermediate Al mask layer and developed by diluted HF solution, Al layer underneath the exposed PS brush was etched directly by HF. Since Al layer underneath unexposed PS was protected from wet etch, the resulting patterns on the Al mask layer showed negative tone behavior.

In Chapter 5, the mixture of PS and PDMS was studied as negative tone e-beam resist with high dry etch resistance. High dry etch resistance is one of the most important characteristics of e-beam resist because resist with high resistance can be used as dry etch mask, and the patterns on the resist can be transferred to the substrate using direct dry etch. Recently, hydrogen silsesquioxane (HSQ) has been vigorously studied as negative tone resist with high dry etch resistance and high resolution. However, it has several drawbacks: it is very expensive, the shelf life is very short, and the processes should be done very quickly to obtain reproducible results. Here, it was demonstrated that PS that contains PDMS can be used as negative tone e-beam resist with high dry etch resistance. It was confirmed that by adding PDMS into PS, the resistance to the dry etch dramatically increased, but the sensitivity and contrast remained nearly the same. Thus, PS-PDMS can be a low-cost replacement of HSQ resist when negative tone e-beam resist with high dry etch resistance is required.

Acknowledgements

First of all, I would like to thank to my family and my friends who always supported and encouraged me throughout my studies.

Also, I would like to express my great appreciation to Professor Bo Cui for his fruitful advices and suggestions on my research work. The completion of this thesis would not have been possible without his tremendous help.

I am also grateful to the members of nanofabrication group at Waterloo, especially to Ripon Dey, Ferhat Aydinoglu, Mohammad Soltani, and Yaoze Liu, with whom I had beneficial discussions and worked together in the cleanrooms.

Dedication

To my family

Table of Contents

AUTHOR'S DECLARATION ii
Abstract iii
Acknowledgements v
Dedication vi
Table of Contents vii
List of Figures ix
List of Tables xii
Chapter 1 Introduction 1
1.1 Introduction to nanotechnology 1
1.2 Objectives 2
1.3 Thesis organization 2
Chapter 2 Electron beam lithography 3
2.1 Overview 3
2.2 Electron beam source 5
2.3 Beam size and aberrations 6
2.4 Interaction of electrons with resist/substrate and electron scattering 9
2.5 Proximity effect 12
2.6 Electron beam resist 13
2.7 Resist coating on non-flat surfaces 18
Chapter 3 Grafted PMMA mono-layer brush as negative tone e-beam resist 20
3.1 Introduction 20
3.2 Experimental 20
3.3 Results and discussion 23
3.3.1 Packing density 23
3.3.2 Solvent development 23
3.3.3 Thermal development 25
3.3.4 Water contact angle measurement 29
3.3.5 Fabrication on Silicon 29
3.3.6 Fabrication on AFM cantilever 34
3.4 Fabrication on fused silica substrate 35
3.5 Summary and conclusions 37

Chapter 4 Grafted polystyrene mono-layer brush as positive and negative tone e-beam resist........... 38
4.1 Introduction........ 38
4.2 Experimental........ 38
4.3 Results and discussion........ 41
4.3.1 Packing density........ 41
4.3.2 Negative tone results........ 41
4.3.3 Positive tone results........ 43
4.4 Summary and conclusions........ 45
Chapter 5 Mixture of polystyrene and PDMS with high dry etch resistance as negative tone e-beam resist for potential HSQ replacement........ 47
5.1 Introduction........ 47
5.2 Experimental........ 48
5.3 Results and discussions........ 49
5.3.1 Sensitivity and contrast curves........ 49
5.3.2 Dry etch resistance........ 50
5.3.3 Line array patterns on Si wafer........ 54
5.4 Summary and conclusions........ 56
Chapter 6 Conclusion........ 57
References........ 60

List of Figures

Figure 2.1 Schematic drawing of electron beam lithography system (Adapted from Ampere A Tseng[1]).....4

Figure 2.2 Monte Carlo simulation of the trajectories of electrons incident on PMMA film on Si substrate at (a) 10 keV and (b) 20keV (Adapted from D. F. Kyser[3]).....10

Figure 2.3 Simulated profile of electron beam exposure and double Gaussian curve fit (Adapted from M. A. McCord[8]).....11

Figure 2.4 Electron distribution on (a) standard substrate; and (b) membrane substrate (Adapted from M. D. Fischbein[9]).....13

Figure 2.5 Schematic of the process using positive and negative resist.....14

Figure 2.6 Contrast curve of positive resist.....15

Figure 2.7 Process to fabricate protruded patterns by: (a) Direct dry etch process; and (b) liftoff process.....16

Figure 2.8 SEM image of 9-nm-pitch nested-L structures on 10-nm-thick HSQ (Adapted from J. K. W. Yang[13]).....17

Figure 3.1 Process steps for patterning substrates using PMMA monolayer brush as negative resist when the sacrificial layer is aluminum. The PMMA can be coated by spin or dip coating, with non-uniform thickness for irregular surfaces. But after washing away the bulk film by acetic acid, the remaining mono-layer brush has very uniform thickness.....21

Figure 3.2 Chemical formula of PMMA-co-PMAA.....22

Figure 3.3 Formation of the bonding between -COOH group in PMMA-co-PMAA and -OH group on the surface of substrate.....22

Figure 3.4 Thickness of PMMA after development and aluminum layer after Al wet etch. Development condition is: (a) MIBK:IPA development for 7 seconds; (b) acetone development for 7 seconds; and (c) without any development. Al wet etch was performed by soaking the film in diluted HF for 11 seconds.....24

Figure 3.5 Thickness of PMMA after 1-minute thermal treatment. The dashed line shows the PMMA thickness before thermal treatment.....26

Figure 3.6 Thickness of PMMA after development and aluminum layer after Al wet etch. Development condition is: (a) Thermal development at 360 °C for 1 minute; and (b) 4 minutes. Al wet etch was performed by soaking the film in diluted HF for 11 seconds. 27

Figure 3.7 Thickness of PMMA after thermal development at 360 °C for 1 minute.......................... 29

Figure 3.8 (a)-(c) SEM images of line arrays fabricated on Si substrate. EBL was carried out at 3 keV. (a) Exposure dose 6,000 μC/cm^2, developed by MIBK:IPA (1:3 volume ratio) for 7 seconds, Al etch by diluted HF for 11 seconds; (b) exposure dose 6,000 μC/cm^2, developed by acetone for 30 seconds, Al etch by diluted HF for 11 seconds; and (c) exposure dose 3,000 μC/cm^2, developed by acetone for 30 seconds, Al etch by PAN etchant for 400 seconds at room temperature. (d) AFM image of line arrays shown in (c). 30

Figure 3.9 SEM images of line arrays etched into silicon and Monte Carlo simulation of electron trajectories. PMMA brush was developed at 360 °C for 1 minute. (a) Line patterns exposed at 3 keV, area dose 3,000 μC/cm^2, width 100 nm, pitch 200 nm; (b) 20 keV, area dose 33,000 μC/cm^2, width 100 nm, pitch 200 nm; (c), (d) Monte Carlo simulation of electron trajectories at (c) 3 keV and (d) 20 keV; (e) line patterns exposed at 3 keV, line dose 20 nC/cm, pitch 100 nm; and (f) 20 keV, line dose 120 nC/cm, pitch 60 nm. 32

Figure 3.10 SEM image of various patterns on silicon substrate. (a) Einstein's picture exposed at 20 keV, 40,000 μC/cm^2, 60 nm pixel size; (b) zoom-in image of (a); (c) geometric pattern expressed by trigonometric function exposed at 20 keV, 200 nC/cm; (d) cycloid pattern exposed at 20 keV, 200 nC/cm; (e) trochoid patterns exposed at 20 keV, 200 nC/cm; and (f) zoom-in image of (e).............. 33

Figure 3.11 (a)(b) SEM images of line arrays etched into silicon. PMMA brush was exposed at 3 keV with area dose of 9,000 μC/cm^2, followed by thermal development of 360 °C for 4 minutes: (a) 1 μm period; and (b) 500 nm period. (c) AFM image of line arrays shown in (b)...................................... 34

Figure 3.12 SEM images of line and geometrical patterns fabricated on non-flat region of an AFM cantilever: (a) top view; (b) zoom-in image of cycloid pattern, 20 keV, 400 nC/cm; (c) zoom-in image of line pattern, 20 keV, 400 nC/cm, period 200 nm. 35

Figure 3.13 (a) SEM image of protruded line arrays fabricated on fused silica substrate, 3 keV, 5,000 μC/cm^2; and (b) the result of AFM measurement of the same patterns. 37

Figure 4.1 Process steps for patterning substrates using polystyrene mono-layer brush for both negative and positive e-beam resist. 40

Figure 4.2 (a)(b) SEM images of protruded line arrays etched into silicon. PS brush was developed thermally at 300 °C for 1 minute: (a) 500 nm period, 2.2 nC/cm; and (b) 1 μm period 3.8 nC/cm. (c) AFM image of the line arrays shown in (b). 43

Figure 4.3 (a)-(c) SEM images of recessed line arrays etched into silicon. PS brush was developed by diluted HF for 15 seconds: (a) 300 nm period, 0.2 nC/cm; (b) 1 μm period 0.2 nC/cm; and (c) 500 nm period, 3.8 nC/cm. (d) AFM image of the line arrays shown in (c). 44

Figure 5.1 Contrast curves of pure PS and the mixture of PS and PDMS exposed at: (a) 20 keV; and (b) 10 keV........ 50

Figure 5.2 Remaining resist thickness after O_2 RIE (pure PS and PS-PDMS, ratio 10:1). 51

Figure 5.3 AFM image of 500-nm-thick PS-PDMS (ratio 10:1) film after 10-minute O_2 RIE. 51

Figure 5.4 SEM images of PS-PDMS after e-beam exposure and 210-second O_2 RIE. The ratio of PS:PDMS is: (a1)-(a4) 10:1; (b1)-(b4) 5:1; and (c1)-(c4) 5:2. The exposure dose is: (a1)(b1)(c1) 150 $\mu C/cm^2$; (a2)(b2)(c2) 98 $\mu C/cm^2$; (a3)(b3)(c3) 64 $\mu C/cm^2$; and (a4)(b4)(c4) 42 $\mu C/cm^2$. 53

Figure 5.5 Etching rate of pure PS and PS-PDMS by deep Si RIE with SF_6 and C_4F_8 gases. 54

Figure 5.6 SEM images of line arrays on 250-nm-thick PS-PDMS (ratio 10:1): (a) Line arrays with 200 nm width, 1μm pitch, exposed at 20 keV, 200 $\mu C/cm^2$; (b) line arrays shown in (a) after 150-second O_2 RIE; and (c) zoom in image of (b). 55

Figure 5.7 SEM images of line arrays on 80-nm-thick PS-PDMS (ratio 5:2) after 210-second O_2 RIE, exposed at 10 keV, 100 $\mu C/cm^2$: (a) 100 nm width; and (b) 250 nm width. The wavy resist structure is caused by capillary force. 55

List of Tables

Table 4.1 Thermal development condition and results. Circle symbols mean patterns are found on substrate after pattern transfer, and cross symbols mean there are no patterns on substrate after pattern transfer. 42

Table 6.1 Advantages and disadvantages of each e-beam resist. 59

Chapter 1

Introduction

1.1 Introduction to nanotechnology

The field of nanotechnology has kept expanding since mid-20th century. As the name suggests, nanotechnology is the field related to nanoscale material. One of the most widely recognized applications of nanotechnology is nanoelectronics, which is the key of the today's electronic devices. However, the applications are not restricted to the field of electronics; nanotechnology is now applied to variety of fields, such as photonics, robotics, and bio and medical fields. Nanofabrication technology is the technology about how to realize the desired structures in nanoscale, and is one of the key technology that supports the rapid growth of nanotechnology. As well as the various application of nanotechnology, nanofabrication itself has been studied for a long time.

There are two major approaches for nanofabrication: top-down fabrication and bottom-up fabrication. In top-down approaches, nanostructures are fabricated by etching out small structures from larger substrates. The fabrication starts from the flat plane of a large block, and then the material that is not required is removed to create desired structures. The most common technologies of top-down approaches are photolithography and electron-beam lithography (EBL). EBL is the direct writing technique that uses electron beam, and it is capable of writing patterns without using any mask. Because of the capability of writing patterns without mask and the high resolution, EBL is widely used both for research purpose and industry, especially for prototyping or mask production that is used in photolithography. Currently, almost all silicon based micro- or nanoelectronics, such as IC or LSI, are fabricated using the top-down approach.

In contrast, molecules or atoms are built up to compose complex nanoscale structures in bottom-up approaches. Self-assembly technique is the most widely used method for bottom-up approaches. Bottom-up approaches have a potential to realize complex three-dimensional structures that are difficult to achieve with top-down approaches.

1.2 Objectives

The objective of the first part of this work is to develop novel electron beam resists that are applicable not only for conventional flat substrates, but also for non-flat, irregular surfaces. As such electron beam resists, the characteristics of monolayer polymer brush including monolayer polystyrene brush and monolayer poly(methyl methacrylate) (PMMA) brush was examined. Also, the process to fabricate nanoscale patterns on substrates using these polymer brushes was developed.

The objective of the second part is to examine the mixture of polystyrene (PS) and polydimethylsiloxane (PDMS) as a novel negative tone e-beam resist with high dry etch resistance.

1.3 Thesis organization

In Chapter 2, the basic principle of electron beam lithography and some of the existing method of resist coating is explained. Chapter 3 and Chapter 4 highlight the experimental results about polymer monolayer brush as e-beam resist. First, PMMA monolayer brush is discussed in Chapter 3, and then PS monolayer brush is discussed in Chapter 4. In Chapter 5, the experimental results of the mixture of PS and PDMS as a negative tone e-beam resist are discussed. Finally, Chapter 6 provides a summary of this thesis.

Chapter 2

Electron beam lithography

2.1 Overview

Electron beam lithography (EBL) is one of the most popular nanopatterning techniques for research and prototyping purposes because of its high resolution and the capability of direct patterning without any mask or mold. However, since the throughput of EBL is very low, it is not suitable for mass production. Therefore, the applications of ELB are generally limited to scientific research and mask production for other lithography techniques, such as photolithography. For the application that requires high throughput, such as semiconductor manufacturing, photolithography (or optical lithography) is widely used.

The mechanism of electron beam lithography system is very similar to that of scanning electron microscope (SEM). Therefore, EBL system was first developed along with the development of SEM in 1960s. Since the mechanisms of EBL and SEM are similar, low-cost EBL systems are achieved by just adding some accessories, such as beam blanker and hardware controller, to existing SEM systems. Such inexpensive EBL systems are popular for research applications. For industrial applications, dedicated e-beam writing systems are used. They can achieve higher reproducibility, automatic and continuous writing, and accurate control of the stage.

As its name suggests, electron beam lithography uses electron beam, whereas photolithography uses UV light to draw patterns. Compared with photolithography, higher resolution can be easily achieved by electron beam lithography because wavelength of electron beam is much smaller than that of UV light. For example, the de Broglie wavelength of electron

beam at 30 keV is only 0.007 nm, thus the diffraction limit is not important for the resolution of electron beam lithography. On the other hand, diffraction is very important factor which determines the resolution in photolithography.

Figure 2.1 shows a schematic drawing of electron beam lithography system. It consists of an electron gun, a beam blanker, and series of electromagnetic lenses and apertures. In general, electron beam emitted from the electron gun is converged on the surface of a sample coated with electron beam resist, and deflected to scan on the resist. When the electron exposure is not needed, the electron beam can be blanked by applying a DC voltage to the beam blanker. Deflected electron beam is blocked by the blanking aperture while the beam blanker is on.

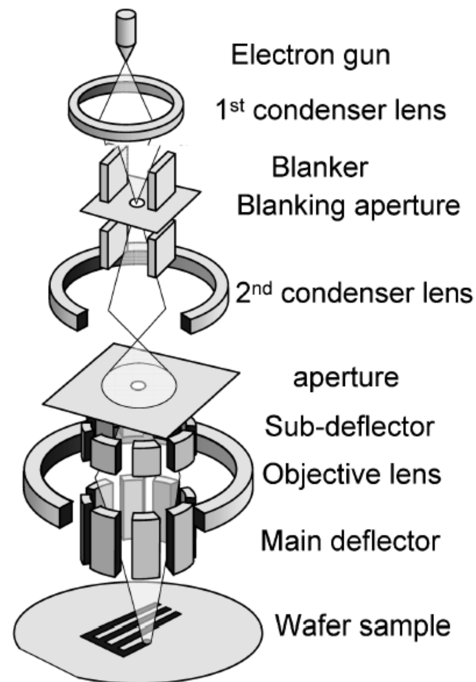

Figure 2.1 Schematic drawing of electron beam lithography system (Adapted from Ampere A Tseng[1]).

2.2 Electron beam source

Electron beam source is one of the most important components of EBL system. There are three types of electron beam source: thermionic emission gun, cold field emission gun, and Schottky gun (field assisted thermionic emission gun). In any types of gun, electrons are emitted from the cathode of the gun. In order for electrons to be emitted, electrons should pass through the potential barrier at the surface of the cathode. Each type of electron gun utilizes different method to pass through the potential barrier.

Thermionic emission gun uses thermal energy to overcome the potential energy. Tungsten (W) and lanthanum hexaboride (LaB_6) are most commonly used filament materials for thermionic emission gun. Tungsten can withstand very high temperature, and it only requires modest vacuum as high as 10^{-5} Torr. One of the main drawbacks of tungsten filament is its low brightness. The tungsten filament is typically heated to about 3,000 K, which gives electrons thermal kinetic energy of about 0.4 eV. Since the work function of tungsten is approximately 4.2 eV, only a few electrons can pass through the potential barrier, which resulted in low brightness. The work function of LaB_6 is about 2.6 eV, so LaB_6 filament can generate higher brightness than tungsten filament. However, it requires higher vacuum around 10^{-6} Torr. Another drawback of thermionic is large source size. Since large area of the filament is heated, electrons are emitted from large area and resulting source size becomes large. Therefore, large demagnification is required to achieve small beam size.

Cold field emission gun uses tunneling effect to pass through the surface potential barrier of a filament. A high voltage is applied to a sharp tip, which creates electric field high enough ($>10^8$ V/cm) to allow electrons to pass through the potential barrier by tunneling effect. Since the tunneling electrons are the main source of electron beam, the emission is independent on the

source temperature. Therefore, it can work at room temperature, and is called “cold” field emission gun. Since the field emission occurs only near the tip apex, beam size of cold field emission is very small compared with that of thermionic gun. However, it requires ultra-high vacuum about 10^{-10} Torr. Main advantages of cold field emission other than small beam size and low operating temperature are high brightness, high current density, low energy spread and long life time of 7 years or longer. However, since it is operated at room temperature, the contaminations easily build up on the cathode, which causes large beam noise and emission current drift. These problems are critical for e-beam lithography, thus the cold field emission gun is not suitable for e-beam lithography systems.

Schottky gun, or a field-assisted thermionic emitter, uses both thermal energy and electric field to give electrons enough energy to pass through the potential barrier. The work function is reduced by the applied field, which helps more electrons get out of the emitter. The tip is coated with low work function material such as zirconia (ZrO_2) to further lower the work function. Even though a Schottky gun is a thermionic emitter, the brightness is comparable with that of cold field emission gun. Also, it only requires high vacuum as high as 10^{-8} Torr, and can produce higher total current compared to cold field emission gun, which makes Schottky gun suitable for electron beam lithography. Since the lifetime of the tip is about 2 years or less, it has to be replaced regularly.

2.3 Beam size and aberrations

The resolution of electron beam lithography is affected by various factors. The spot size of electron beam is one of the most important factors because patterns smaller than the beam spot size cannot be written. The dominant factors that determine the beam spot size in commercial EBL system is virtual source size and demagnification. If the lenses were ideal lenses without any

aberrations and there was no beam spread because of repelling force between electrons, the electron beam diameter on the writing surface would be expressed as:

$$d_{\mathrm{g}} = \frac{d_{\mathrm{v}}}{M},$$

where d_{v} is the virtual source diameter, M (>1) is demagnification.

However, real lenses (in this case electromagnetic lenses) have various aberrations, so the actual beam diameter always becomes larger than the ideal one. Spherical aberration, chromatic aberration, astigmatism and diffraction have to be considered in the real situation.

Spherical aberration occurs because of finite angular divergence of the beam. Electrons passing through points on lenses near the axis (paraxial electrons) are focused at slightly different place from those passing through points far from the axis (peripheral electrons). Therefore, when electron beam has angular divergence, even a point source cannot be focused to another point. The amount of spherical aberration is expressed as:

$$d_{\mathrm{s}} = \frac{1}{2} C_{\mathrm{s}} \alpha^3,$$

where C_{s} is the coefficient of spherical aberration, α is the beam semi-angle.

Chromatic aberration is caused by energy distribution of electron beam. The focal length of electromagnetic lenses depends on the energy of electrons, so the energy spread of electron beam causes aberration. The amount of chromatic aberration is expressed as:

$$d_{\mathrm{c}} = C_c \frac{\Delta E}{E_0} \alpha,$$

where C_{c} is the coefficient of chromatic aberration, ΔE is the energy spread of electron beam, and E_0 is the mean energy of electron beam. Chromatic aberration becomes higher when lower energy

electron beam is used or electron source with larger energy spread such as thermionic gun is used.

Astigmatism is caused by the different focal points of electrons propagating in two perpendicular planes. Astigmatism can be removed by adjusting a stigmator which imposes a weak electronic or magnetic quadrupole field on the electron beam. When the stigmator is optimized, the spot size broadening due to astigmatism is negligible.

Diffraction is caused by the wave nature of electron. The de Broglie wavelength of electron is written as:

$$\lambda = \left(\frac{h^2}{2mE}\right)^{\frac{1}{2}} = \frac{1.2}{\sqrt{V}}\ \mathrm{nm},$$

where h is the Plank constant, m is the mass of electron, E is the electron energy, and V is the acceleration voltage of the electron in unit of volt. For example, the de Broglie wavelength of the electron with the energy of 30 keV is 0.007 nm. The spot size broadening due to diffraction is written as:

$$d_{\mathrm{d}} = 0.61\frac{\lambda}{\alpha}.$$

Unlike spherical aberration and chromatic aberration, the spot size broadening due to diffraction becomes larger when the beam angle α is smaller. Therefore, diffraction becomes the dominant factor when the angle is very small.

The total beam spot diameter is written as:

$$d = \sqrt{d_{\mathrm{g}}^2 + d_{\mathrm{s}}^2 + d_{\mathrm{c}}^2 + d_{\mathrm{d}}^2}.$$

For typical conditions using field emission gun, the beam size of < 5 nm can be easily achieved. Therefore, the pattern resolution is not limited by beam spot size, but by other factors such as back and forward scattering of electrons, proximity effect, or resist characteristics.

2.4 Interaction of electrons with resist/substrate and electron scattering

When electron beam enters a sample, a series of elastic and inelastic collisions between electrons and atoms in the sample happen. Elastic scattering only changes trajectories of the electrons without losing their kinetic energy. On the other hand, electrons which go through inelastic scattering lose their kinetic energy, and generate other electrons or photons, such as x-rays, auger electrons, and secondary electrons.

Elastic scattering occurs when the incoming electrons hit a nucleus of atoms in the sample. Since the direction of electron changes largely, it is called backscattering. The fraction of electrons which undergo backscattering is roughly independent of electron energy[2], but it depends on the substrate material. Since atoms with a larger atomic number have larger cross-sectional area, backscattering occurs more frequently in material with larger atomic number. Back-scattered electrons can reach areas far away from the incident beam.

The inelastic scattering process is due to electron-electron interactions. Primary electrons are deflected by a small angle and lose their kinetic energy during the interaction with another electron. Therefore, as the primary electrons propagate in resist or substrate, they continue to lose their energy and the beam spot size increases. At the same time as the electrons lose their energy, they generate photons or electrons such as x-rays, auger electrons, and secondary electrons.

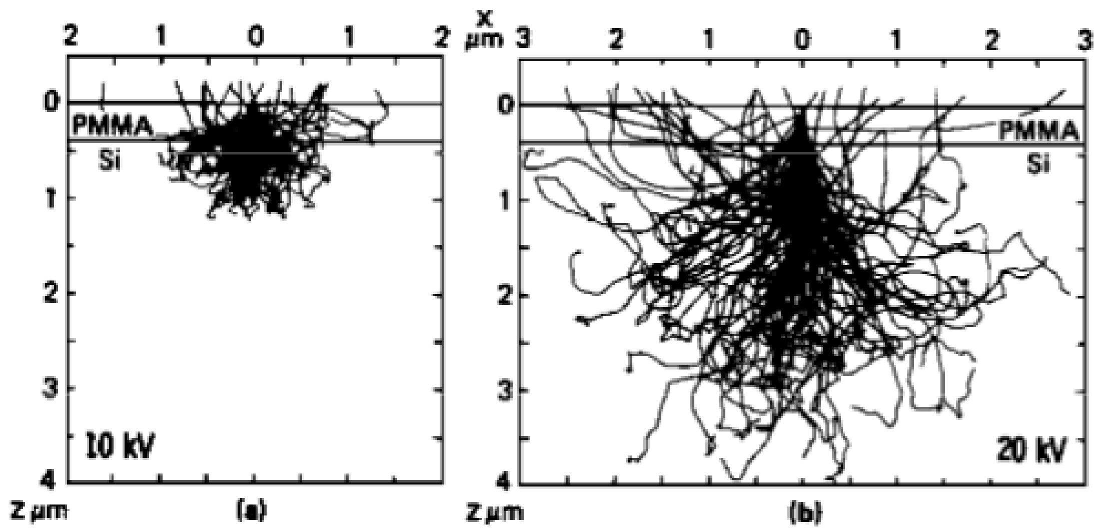

Figure 2.2 Monte Carlo simulation of the trajectories of electrons incident on PMMA film on Si substrate at (a) 10 keV and (b) 20keV (Adapted from D. F. Kyser[3]).

Figure 2.2 shows the simulated trajectories of electrons incident on PMMA film on Si substrate. Electron beam is broadened by both forward and backscattering. Also, electron beam with higher energy can penetrate deeper in the substrate. Therefore, electron beam with higher energy can go farther after backscattering occurs, and causes exposure in the areas far away from the point of incidence. The electron distribution after forward and backscattering is expressed as a sum of two Gaussian distributions[4,5]:

$$f(r) = \frac{1}{1+\eta}\left\{\frac{1}{\pi\alpha^2}\exp\left(-\frac{r^2}{\alpha^2}\right) + \frac{\eta}{\pi\beta^2}\exp\left(-\frac{r^2}{\beta^2}\right)\right\},$$

where r is the distance from the center of incident beam, the first term expresses the forward scattering, and the second term expresses the backscattering, η is the ratio of the backscattering to forward scattering, α is the range of forward scattering, and β is the range of backscattering.

Typically, the forward scattering coefficient α is the order of 10 nm, and the backscattering coefficient β is the order of 1 μm, but these values depend on various factors such as electron beam energy, substrate and resist materials. For example, the higher the electron beam energy is, the shorter the forward scattering range α becomes and the longer the backscattering range β becomes[6].

Figure 2.3 shows the comparison between double Gaussian curve fitting and Monte Carlo simulation of electron beam exposure. The simulated result is well reproduced by the double Gaussian curve fitting in the short range where forward scattering is dominant and in the long range where backscattering is dominant. However, the model fails to reproduce the intermediate range. It was shown that more accurate results can be achieved by adding extra Gaussian or exponential terms to the double Gaussian distribution[7]. These models are used for a proximity effect correction, which is described in the next section. For many cases, double Gaussian distribution provides sufficiently accurate results. When more accurate calculation is required, the models with extra Gaussian or exponential terms are used at the cost of calculation time.

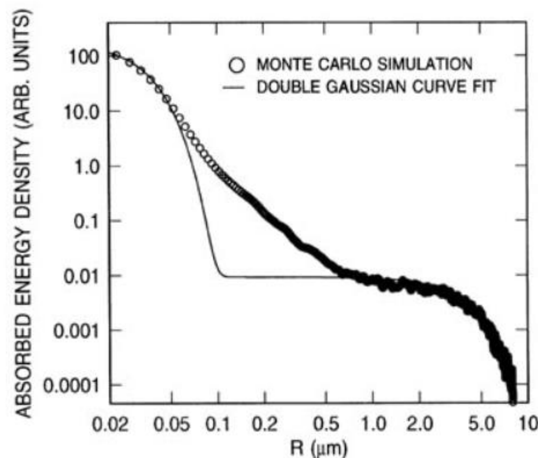

Figure 2.3 Simulated profile of electron beam exposure and double Gaussian curve fit (Adapted from M. A. McCord[8]).

2.5 Proximity effect

Since the energy of incident electron beam is too high to cause chain-scission or cross-linking to resist, secondary electrons with several electron volts are responsible for most resist exposure. These secondary electrons are generated by forward scattering of incident electron beam, and these secondary electrons play main role to expose resist. In addition to incident electrons, backscattered electrons can also be the source of secondary electrons. Since the backscattered electrons can reach the areas far from the point of electron incidence, resist in those areas is also exposed to electron beam, which is called proximity effect.

Typically, proximity effect is negligible for isolated or sparse patterns, but not negligible for dense patterns. Proximity effect can be beneficial for some cases, such as exposure of large area. Even if the beam spot size is about a few nanometers, the step size of a few tens of nanometers is typically enough to achieve uniform exposure because of proximity effect. However, when dense and fine structures patterns are exposed, proximity effect causes a severe problem.

There are several methods to reduce proximity effect for dense and fine patterns. Since the proximity effect is caused by electrons back-scattered in substrate, the use of membrane substrate greatly helps to reduce the proximity effect as shown in Figure 2.4. For example, very small gaps less than a few nanometers were demonstrated by using PMMA on 100-nm-thick Si_3N_4 membrane[9]. Another way to reduce proximity effect is a proximity effect correction. The proximity effect is calculated based on double Gaussian distribution or other numerical models, and the exposure patterns and doses are modified to compensate the proximity effect.

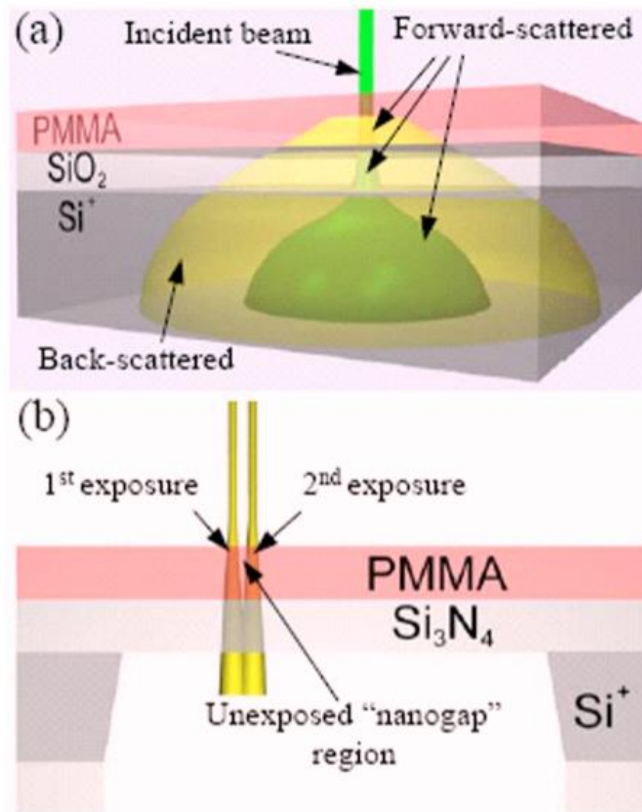

Figure 2.4 Electron distribution on (a) standard substrate; and (b) membrane substrate (Adapted from M. D. Fischbein[9]).

2.6 Electron beam resist

Electron beam resists can be classified as positive and negative resists depending on the response to the e-beam exposure. Figure 2.5 shows the schematic of the processes using positive and negative resists. When positive tone resist is used, the area exposed to electron beam becomes more soluble, so the exposed area is removed during the development process. On the other hand, interaction with electron beam renders negative tone resist less soluble. Therefore, the exposed area remains after development when negative tone resist is used.

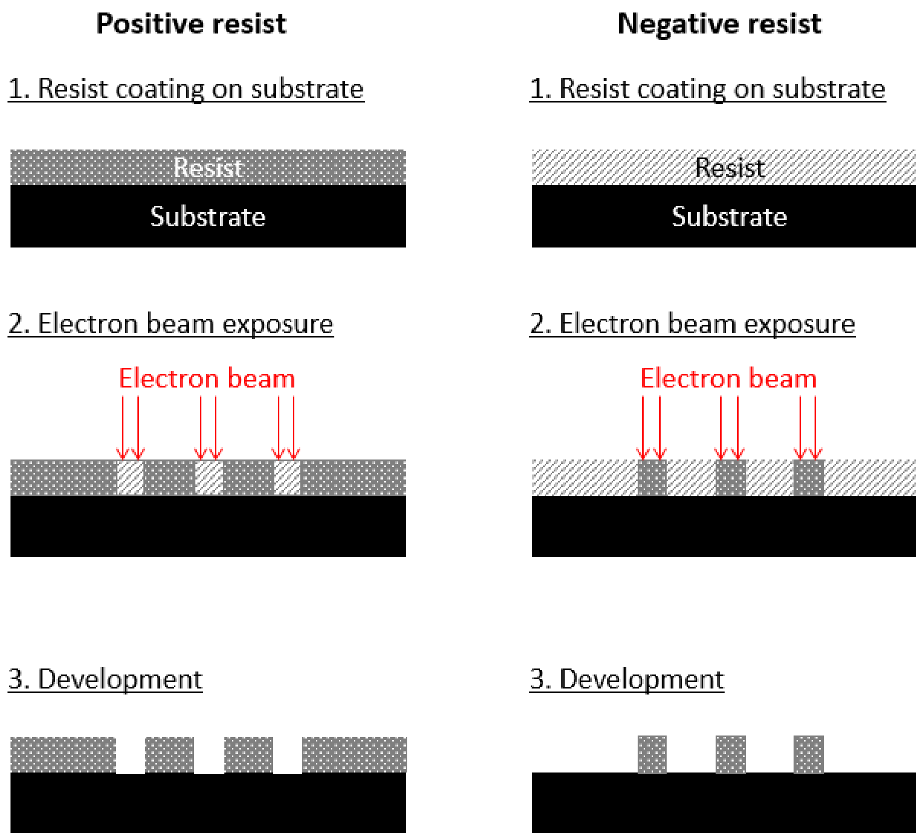

Figure 2.5 Schematic of the process using positive and negative resist.

The most important characteristics of resist are contrast, sensitivity and resistance to dry etch. Sensitivity is defined as the minimum dose necessary to fully expose the resist. Figure 2.6 shows the relationship between exposure dose and remaining resist thickness after development of positive tone resist. This curve is called a contrast curve, and sensitivity is indicated as D_1. Sensitivity depends on various factors including electron energy, the size of the patterns, substrate material, and development condition. For example, higher exposure dose is required when electron beam with higher energy is used.

Contrast indicates how sharp the patterns on resist can be. It is defined as a slope of the contrast curve:

$$\gamma = \frac{1}{\log\left(\frac{D_1}{D_0}\right)}.$$

Generally, resist with higher sensitivity has lower contrast, and vice versa.

Resistance to dry etch is also an important characteristic of resist because dry etch is widely used to transfer the pattern on resist into the substrate. If the resistance to dry etch of the resist is high enough, substrate can be etched using the resist as a dry etch mask as shown in Figure 2.7 (a). If liftoff process shown in Figure 2.7 (b) is used, high resistance to dry etch is not necessary.

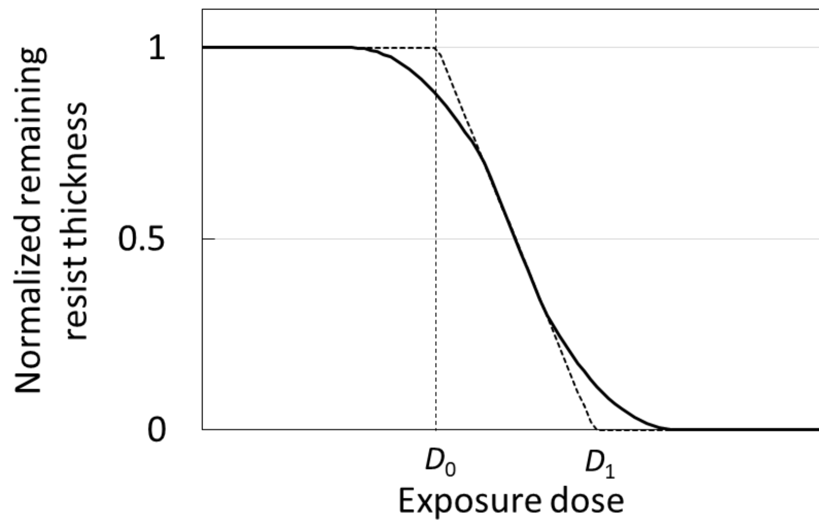

Figure 2.6 Contrast curve of positive resist.

(a) Direct dry etch using negative resist

1. Resist coating on substrate

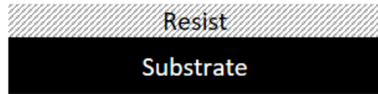

2. Electron beam exposure

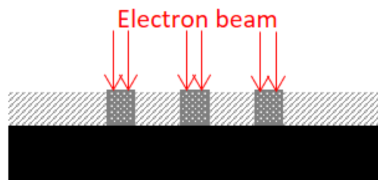

3. Development

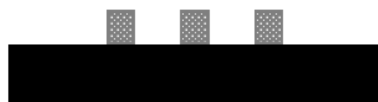

4. Dry etch

(b) Liftoff using positive resist

1. Resist coating on substrate

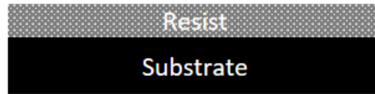

2. Electron beam exposure

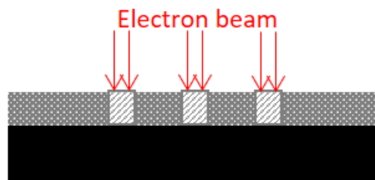

3. Development

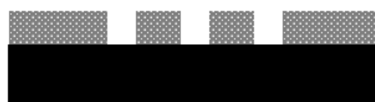

4. Metal deposition

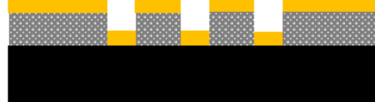

5. Liftoff

6. Dry etch

Figure 2.7 Process to fabricate protruded patterns by: (a) Direct dry etch process; and (b) liftoff process.

The most common example of positive tone resist is PMMA. PMMA has been used most widely since its discovery in 1968[10]. PMMA consists of very long chains of polymer, and undergoes chain-scissions when it is exposed to electron beam. It has relatively high contrast typically about γ=5-10, thus it is good for fine patterns. Another example of positive resist is ZEP520A. ZEP520A has been developed as a replacement for PMMA with higher sensitivity and higher dry etch resistance[11].

Hydrogen silsesquioxane (HSQ) is an inorganic negative tone resist first studied by Frye and Collins[12]. The resolution and sensitivity are similar to those of PMMA. 9-nm-pitch nested-L structures were demonstrated by Yang by using 10-nm-thick HSQ as shown in Figure 2.8[13]. HSQ has high resistance to dry etch because it is silicon dioxide based material, so it can be used as hard mask for dry etch. The drawback of HSQ is its instability. All the processes from resist coating to development need to be performed quickly to obtain reproducible results; otherwise, HSQ absorbs contaminants, which deteriorates the quality of HSQ[14,15]. Polystyrene can also be used as negative tone resist. Polystyrene shows high contrast comparable to those of ZEP or PMMA[16].

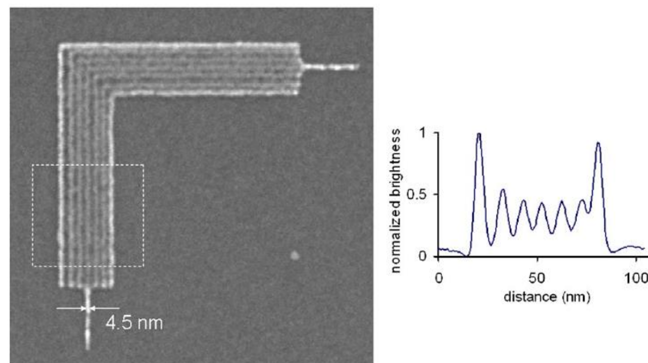

Figure 2.8 SEM image of 9-nm-pitch nested-L structures on 10-nm-thick HSQ (Adapted from J. K. W. Yang[13]).

2.7 Resist coating on non-flat surfaces

Spin coating is the most popular resist coating method. Since it is very simple and the resulting film is very uniform, spin coating is widely used for both research and industrial purposes. The thickness of the film depends on spinning condition such as rotation speed, rotation time, and the viscosity and concentration of the resist solution. However, spin coating is not suitable for non-flat or irregular surfaces because spin-coated film on the irregular surfaces is not uniform.

There is a great demand for nanofabrication on non-flat or irregular surfaces because it has promising applications such as nanofabrication on AFM tips and fiber tips, which can be used for tip-enhanced Raman spectroscopy[17] and chemical and biological sensors based on localized surface plasmon resonances[18], respectively. Therefore, several resist coating methods for unconventional substrates have been demonstrated, which include ice lithography[19,20], evaporative resists[21,22], spray coating[23], spin coating using low viscosity resists[24,25], float coating[26], and dip coating[27].

In ice lithography, water ice deposited on substrates is used as e-beam resist. It is applicable on non-flat surfaces, and nanofabrication on AFM tips was demonstrated as an example[19]. However, the ice lithography has several drawbacks; it requires a specially modified SEM system, and sensitivity of the resist is extremely low. Another method of resist coating is thermal evaporation. Some e-beam resists can be thermally evaporated and coated on irregular surfaces to be used as e-beam resist. For example, polystyrene has been demonstrated as evaporated e-beam resist[21,22]. However, only the limited types of e-beam resist can be coated using this method. One example of the resists that is not suitable for evaporation is PMMA, which is very commonly used positive e-beam resist. In order to be thermally evaporated, thermal decomposition process of the resist should include random chain scission that occurs in the

middle of the chain. The resist whose thermal decomposition process only consists of end-chain scission, such as PMMA, cannot be coated by thermal evaporation. Spray coating is another way to coat resist on irregular surfaces. When it is applied to sharp trenches, even very sharp edges can be coated[23]. However, the thickness of the film is different on flat area and slanted area.

Also, spin coating is applicable for non-flat surfaces when low viscosity and low surface tension solvent is used for resist coating. It was demonstrated that resist was coated even on vertical surfaces[24,25]. However, in order to apply this method, vertical surfaces should be along the radial direction of the spin. Float coating can also provide uniform film on irregular surfaces. Resist is first floated and dried on water in which a substrate is soaked, and then water is extracted until the resist reaches the top surface of the substrate[26]. Since the resist film is flexible to some extent, it can fit non-flat surfaces. Although it works well for relatively large structure, it is difficult to cover very small structures, such as small holes. Dip coating is also applicable for irregular surfaces, but it is difficult to achieve uniform film with this method[27].

Chapter 3

Grafted PMMA mono-layer brush as negative tone e-beam resist

3.1 Introduction

As a new resist coating method that is applicable to non-flat surfaces, the process using monolayer polymer brush as e-beam resist has recently been developed[28]. Polymer brushes are long chains of polymers one end of which is attached to a surface or interface, with chain length longer than the distance between adjacent grafting points[29,30]. The name "brush" refers to bristles on a brush. Nanofabrication on AFM tips was demonstrated using monolayer PMMA brush as positive e-beam resist. Although it is well known that PMMA can work as negative e-beam resist when it is exposed to very high dose electron beam[31,32], monolayer PMMA brush has only been used as positive resist. Since PMMA brush is strongly connected to substrate via chemical bonding, unexposed area of PMMA brush cannot be removed by solvent, as needed for negative tone.

In this study, it is shown that monolayer PMMA brush can be used as negative e-beam resist. Instead of solvent development, thermal development is used to achieve negative tone. Negative resist is needed when patterning sparse protruded structures, for which the exposure time would be too long if using positive resist.

3.2 Experimental

Figure 3.1 shows the schematic diagram of the fabrication process to fabricate protruded structures on substrate by using monolayer PMMA brush as negative e-beam resist. The PMMA brush is grafted onto a substrate in the same way as previous work[28]. First, a sacrificial metal layer (8-10 nm Al or Cr layer) for pattern transfer is coated on the substrate because monolayer

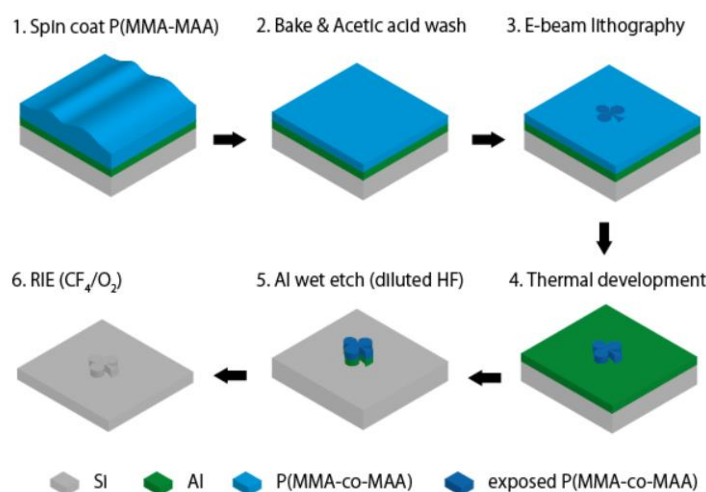

Figure 3.1 Process steps for patterning substrates using PMMA monolayer brush as negative resist when the sacrificial layer is aluminum. The PMMA can be coated by spin or dip coating, with non-uniform thickness for irregular surfaces. But after washing away the bulk film by acetic acid, the remaining mono-layer brush has very uniform thickness.

of PMMA is too thin to transfer pattern directly into substrate. Then, PMMA containing 1.6% methacrylic acid (PMMA-co-PMAA, Mw=34 kg/mol, Mn=15 kg/mol, Sigma-Aldrich Co. LLC) is spin coated on substrate. As shown in Figure 3.2, PMMA-co-PMAA contains carboxyl (-COOH) group. The –COOH group in MAA reacts with the –OH group on the substrate with the release of water during the annealing at 160 °C for 24 hours as shown in Figure 3.3. The bulk of PMMA is then removed by soaking the substrate in acetic acid for 1 minute. Since the bottom layer of PMMA is bonded to the substrate strongly, a grafted monolayer of PMMA remains on the substrate even after the acetic acid wash. Then, electron beam exposure is performed with the electron energy of 3 or 20 keV using RAITH150 Two (Raith GmbH) or LEO 1530 field emission SEM (Carl Zeiss) integrated with the nanometer pattern generation system (JC Nabity Lithography Systems). Although solvent, such as acetone, is used to develop thick PMMA as

negative e-beam resist, solvent development does not work for monolayer PMMA brush. Thus, the brush layer is developed thermally instead of solvent development. When polymers are heated, they undergo thermal decomposition, such as end-chain scission or random-chain scission[33]. Since cross-linked polymer has higher thermal stability than uncross-linked one, cross-linked one needs higher temperature to be vaporized. Therefore, at a proper temperature, only uncross-linked polymer is vaporized and cross-linked one remains. After thermal development, the patterns on monolayer PMMA is transferred to the sacrificial metal layer by wet etching, followed by dry etching of the substrate. The results were compared with those obtained by solvent development.

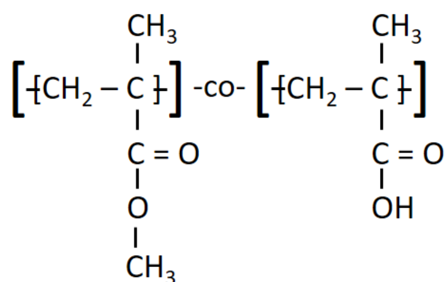

Figure 3.2 Chemical formula of PMMA-co-PMAA.

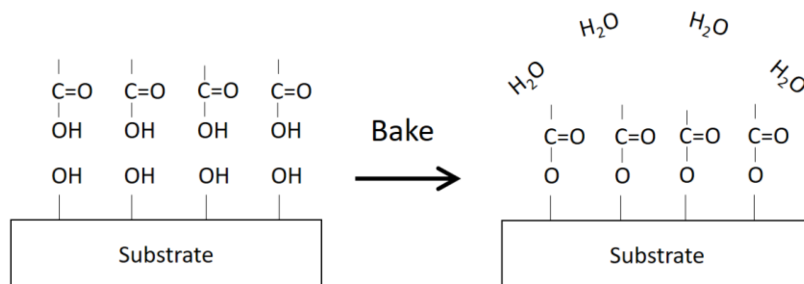

Figure 3.3 Formation of the bonding between -COOH group in PMMA-co-PMAA and -OH group on the surface of substrate.

3.3 Results and discussion

3.3.1 Packing density

The packing density is written as:

$$\sigma = \frac{h\rho N_{\mathrm{A}}}{M_{\mathrm{n}}},$$

where h is thickness, ρ is bulk density of polymer (1.18 g/cm^3 for PMMA), N_{A} is Avogadro number, and M_{n} is number average molecular weight. The thickness of monolayer PMMA brush was measured 8 nm using AFM, so the packing density is calculated as σ=0.38 chains/nm^2. Therefore, the PMMA is in the "brush regime", where the distance between adjacent grafting points is smaller than the chain end-to-end distance[30].

3.3.2 Solvent development

We examined various development method including solvent development and thermal development to determine which development method is suitable for monolayer PMMA brush as negative tone e-beam resist. First, we examined solvent development. We exposed arrays of 5 μm squares at 3 keV with doses from 2 to 10,000 μC/cm^2 on monolayer PMMA brush grafted on aluminum layer. Then, the film was developed in different solvent, MIBK:IPA (1:3 volume ratio) for 7 seconds or acetone for 7 seconds. After development, aluminum wet etch was performed by soaking the film for 11 seconds in diluted HF solution ($HF:H_2O$=1:250 volume ratio). Finally, the residual PMMA layer was etched with O_2 plasma RIE for 10 seconds (20 sccm O_2, 20 mTorr pressure, 20 W RF power). The thickness of the PMMA layer after development and the aluminum layer after the pattern transfer to Al layer were measured with AFM. Figure 3.4 (a) and (b) show the result of MIBK:IPA development and acetone development respectively. For both MIBK:IPA

and acetone development, monolayer PMMA brush worked in a positive tone at low dose, but it got cross-linked and became insoluble when dose was as high as 1,000 μC/cm^2.

However, once the pattern on PMMA was transferred to the aluminum layer, the negative-like behavior of PMMA brush at high dose disappeared. Even though PMMA brush layer remained when the dose was very high, the aluminum layer underneath the highly exposed PMMA was etched away by diluted HF. This result suggests that the PMMA brush developed by solvent cannot be used for etching mask as a negative resist.

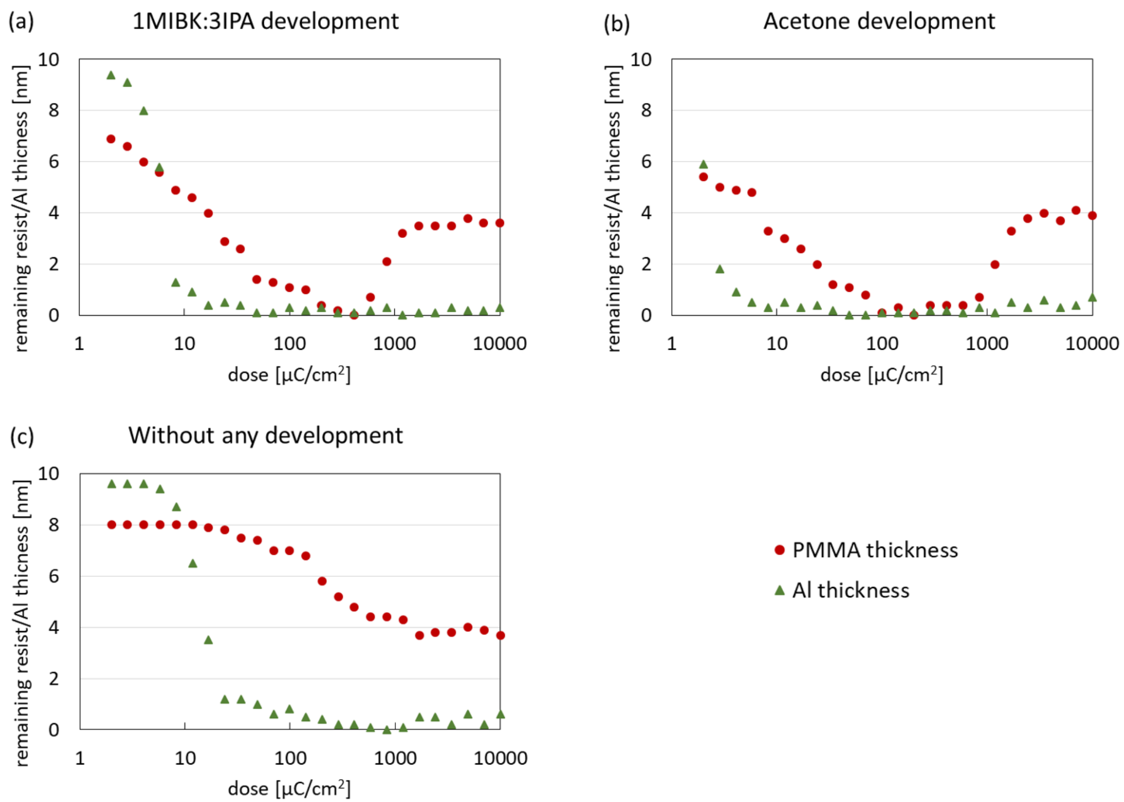

Figure 3.4 Thickness of PMMA after development and aluminum layer after Al wet etch. Development condition is: (a) MIBK:IPA development for 7 seconds; (b) acetone development for 7 seconds; and (c) without any development. Al wet etch was performed by soaking the film in diluted HF for 11 seconds.

Also, the thickness of PMMA and aluminum layer of the sample without any development was measured. The thickness of PMMA was measured after e-beam exposure, and the thickness of Al was measured after soaking film into diluted HF and etching away PMMA by O_2 RIE. Figure 3.4 (c) shows the measured thickness of undeveloped sample. PMMA shrinkage was seen when the dose was higher than 20 $\mu C/cm^2$; but even at 10,000 $\mu C/cm^2$, approximately 4 nm of PMMA remained. Such shrinkage is due to the formation of vaporized material induced by electron beam. Although there was still PMMA layer left, aluminum layer under PMMA exposed to electron beam was etched away by diluted HF. It means that PMMA exposed to electron beam cannot prevent the underneath aluminum layer from being etched by HF. Therefore, PMMA brush does not work as negative e-beam resist when solvent development is performed even though highly exposed PMMA remains after development.

3.3.3 Thermal development

Next, we examined the effect of thermal development. In order to figure out the optimal temperature for thermal development, we first checked the evaporation rate of thick P(MMA-co-MAA) film at various temperatures. The film of P(MMA-co-MAA) was prepared in the same way as PMMA brush, but after baking the film for 24 hours, the bulk of PMMA was not removed. Therefore, there are both grafted PMMA layer and unbonded layers. Thermal decomposition process is the same for both grafted layer and unbonded layers of PMMA; it mainly consists of end-chain scissions[33].

The film was put on a hotplate with a temperature from 250 °C to 370 °C for 1 minute. The thickness of PMMA film before and after thermal treatment was measured by AFM. Figure 3.5 shows the PMMA thickness after thermal treatment. The thickness did not change when the

temperature was less than 320 °C; but it decreased when the film was heated to 340 °C or higher. Therefore, 340 °C or higher temperature is required to develop PMMA.

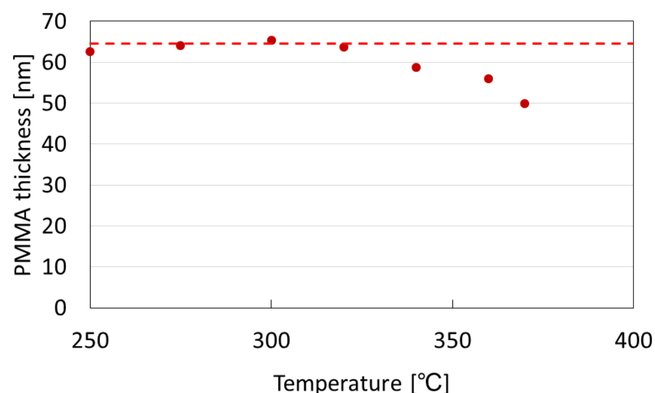

Figure 3.5 Thickness of PMMA after 1-minute thermal treatment. The dashed line shows the PMMA thickness before thermal treatment.

Then, the thickness of PMMA brush after thermal development and the aluminum layer after wet etch were measured in the same way as the film developed by solvents. Thermal development was performed at 360 °C for 1 minute and 4 minutes. The measured thickness is shown in Figure 3.6. When the film was thermally developed for 1 minute, lightly exposed PMMA and heavily exposed PMMA remained and only moderately exposed (about 100 $\mu C/cm^2$) PMMA was removed, similar to the result of solvent development. However, unlike the PMMA brush developed by solvents, the aluminum layer under heavily exposed PMMA was not removed by diluted HF. The result indicates that thermal treatment recovers the resistance of PMMA to wet etch since heavily exposed PMMA without any development cannot protect Al from wet etch. A possible reason is that thermal treatment makes PMMA film denser, which prevents HF from

reaching the underneath Al layer. Therefore, thermally developed PMMA brush can be used as negative e-beam resist.

Since the aluminum layer underneath non- or lightly exposed PMMA also remained after wet etch of aluminum, the result was not completely negative behavior. Completely negative behavior can be achieved by increasing the thermal development time. As shown in Figure 3.6 (b), lightly exposed PMMA was decomposed when longer thermal development was conducted, and the aluminum layer underneath it was etched away. The aluminum layer beneath unexposed PMMA was also confirmed to be removed by diluted HF. Therefore, the monolayer PMMA brush works in a complete negative tone when it is developed at 360 °C for 4 minutes. However, since the thickness of heavily exposed PMMA also decreased, the sensitivity of the resist became lower.

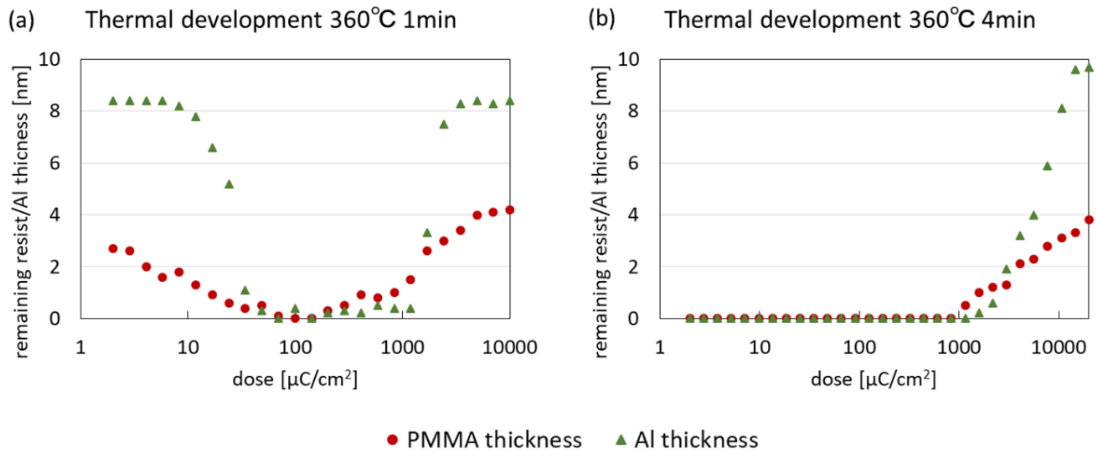

Figure 3.6 Thickness of PMMA after development and aluminum layer after Al wet etch. Development condition is: (a) Thermal development at 360 °C for 1 minute; and (b) 4 minutes. Al wet etch was performed by soaking the film in diluted HF for 11 seconds.

Another way to achieve complete negative behavior is to expose the entire film with UV light before e-beam exposure. It is known that PMMA absorbs deep-UV light shorter than 260 nm[34,35], which results in the chain scissions in PMMA. Therefore, by combining UV exposure of the entire area of PMMA film and e-beam exposure of small patterns, it is expected that even the PMMA film that is not exposed to electron beam will be decomposed easily by thermal development.

As a proof of concept, UV exposure treatment was performed on thick PMMA film (50 nm thick). The film of P(MMA-co-MAA) was prepared in the same way as PMMA brush, but after baking the film for 24 hours, the bulk of PMMA was not removed. Then, the PMMA film was exposed to 185 nm UV light for 30 minutes by using UV ozone cleaner (Novascan, PSDP-UV8). EBL of 5-μm square arrays was carried out after UV ozone treatment at 3 keV with doses from 2 to 6,000 μC/cm^2. Finally, thermal development at 360 °C for 1 minute was performed and the remaining PMMA thickness was measured by AFM.

Figure 3.7 shows the remaining PMMA thickness after thermal development. Because of the UV exposure, lightly exposed area was completely vaporized during the thermal development. The area unexposed to electron beam was also decomposed during the thermal development. Therefore, PMMA film behaved as completely negative tone resist.

We also performed 30-minute UV ozone treatment for PMMA brush followed by EBL and thermal development, but even highly exposed PMMA was decomposed during the thermal development. Since PMMA brush is thinner than bulk PMMA film, exposure time to UV ozone reduced to achieve negative tone behavior.

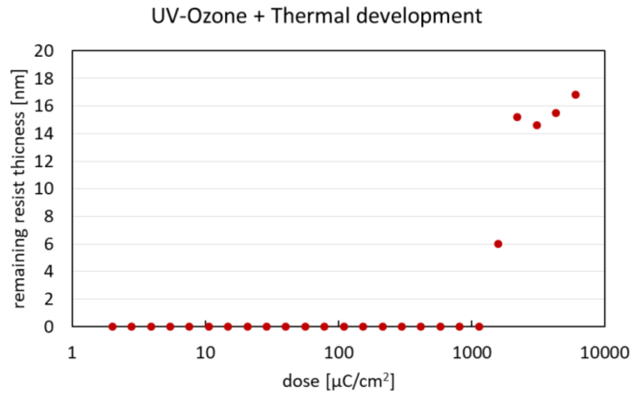

Figure 3.7 Thickness of PMMA after thermal development at 360 °C for 1 minute.

3.3.4 Water contact angle measurement

In order to evaluate the film characteristics toward water, water contact angle measurement was performed for both unexposed and exposed PMMA brush. Contact angle goniometer (ramé-hart instrument co., ramé-hart Model 190) was used to measure the contact angle. The measured contact angle for both unexposed and exposed (300 $\mu C/cm^2$ at 3 keV) PMMA brush were 70 degree, and there was no significant difference between them.

3.3.5 Fabrication on Silicon

Figure 3.8 (a)-(c) show SEM images of line arrays fabricated on Si substrates by using solvent development. EBL was carried out at 3 keV, then PMMA brush was developed by acetone or MIBK:IPA. Since the film was developed by solvent, it behaved as positive tone resist even at very high dose. Al wet etch was performed by diluted HF or PAN etchant (mixture of phosphoric acid, acetic acid and nitric acid) at room temperature. Finally, Si substrate was etched by CF_4/O_2 RIE for 1 minute (20 sccm CF_4, 4 sccm O_2, 10 mTorr pressure, 50 W RF power). Figure 3.8 (d) shows the result of AFM measurement of line arrays shown in Figure 3.8 (c).

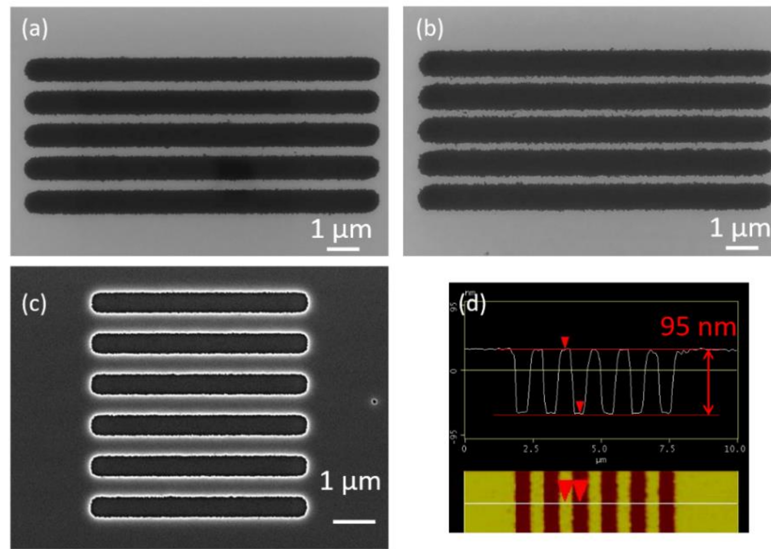

Figure 3.8 (a)-(c) SEM images of line arrays fabricated on Si substrate. EBL was carried out at 3 keV. (a) Exposure dose 6,000 μC/cm^2, developed by MIBK:IPA (1:3 volume ratio) for 7 seconds, Al etch by diluted HF for 11 seconds; (b) exposure dose 6,000 μC/cm^2, developed by acetone for 30 seconds, Al etch by diluted HF for 11 seconds; and (c) exposure dose 3,000 μC/cm^2, developed by acetone for 30 seconds, Al etch by PAN etchant for 400 seconds at room temperature. (d) AFM image of line arrays shown in (c).

Figure 3.9 shows the SEM images of line arrays etched into silicon fabricated using PMMA brush as negative resist. EBL was carried out at 3 or 20 keV, followed by thermal development at 360 °C for 1 minute. In order to perform pattern transfer, 8-10 nm Al sacrificial layer was etched by diluted HF (1:250 dilution ratio), and then silicon substrate was etched by CF_4/O_2 RIE for 1 minute (20 sccm CF_4, 4 sccm O_2, 10 mTorr pressure, 50 W RF power). Since 1-minute thermal development is not enough to fully vaporize unexposed PMMA brush, the results were not completely negative behavior. With the electron energy of 3 keV, only a thin frame surrounding the exposed area was etched away because of small proximity range that exposed the frame area

with a moderate dose, as shown in Figure 3.9 (a). In contrast, with the electron energy of 20 keV, large area around the exposed area was etched because of larger proximity range as shown in Figure 3.9 (b). However, even at 20 keV, the area far away from the exposed area was not etched (not shown in the figure). Figure 3.9 (c) and (d) show the results of Monte Carlo simulation of electron trajectories in PMMA brush on Si with electron energy of 3 keV and 20 keV, respectively. The simulation was performed using Casino v3 (University of Sherbrooke), the freely available software to obtain the electron trajectories based on Monte Carlo modeling. The simulation results show that the proximity range is the order of 100 nm for 3 keV, and a few microns for 20 keV. As shown in Figure 3.9 (e) and (f), line arrays on silicon substrate with 14 nm width and 100 nm pitch, and 20 nm width and 60 nm pitch were obtained with 20 nC/cm at 3 keV, and 120 nC/cm at 20 keV respectively.

Figure 3.10 shows some other patterns made on Si substrate by this process. The patterns on Si substrate have rough line edge because of the lateral etching of the intermediate Al mask layer. In order to avoid the lateral etching, thinner Al layer can be used to make wet etching time shorter. Also, Al layer can be etched by dry etch instead of wet etch for future work.

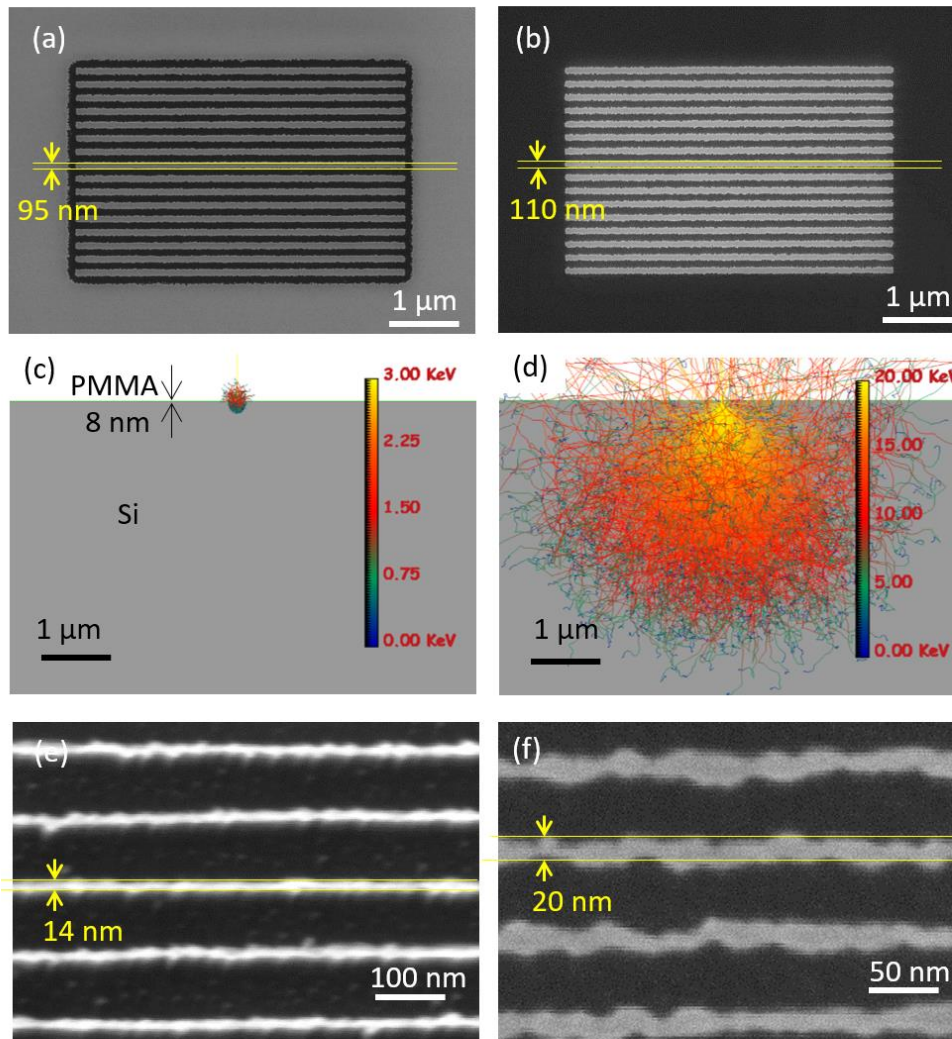

Figure 3.9 SEM images of line arrays etched into silicon and Monte Carlo simulation of electron trajectories. PMMA brush was developed at 360 °C for 1 minute. (a) Line patterns exposed at 3 keV, area dose 3,000 μC/cm^2, width 100 nm, pitch 200 nm; (b) 20 keV, area dose 33,000 μC/cm^2, width 100 nm, pitch 200 nm; (c), (d) Monte Carlo simulation of electron trajectories at (c) 3 keV and (d) 20 keV; (e) line patterns exposed at 3 keV, line dose 20 nC/cm, pitch 100 nm; and (f) 20 keV, line dose 120 nC/cm, pitch 60 nm.

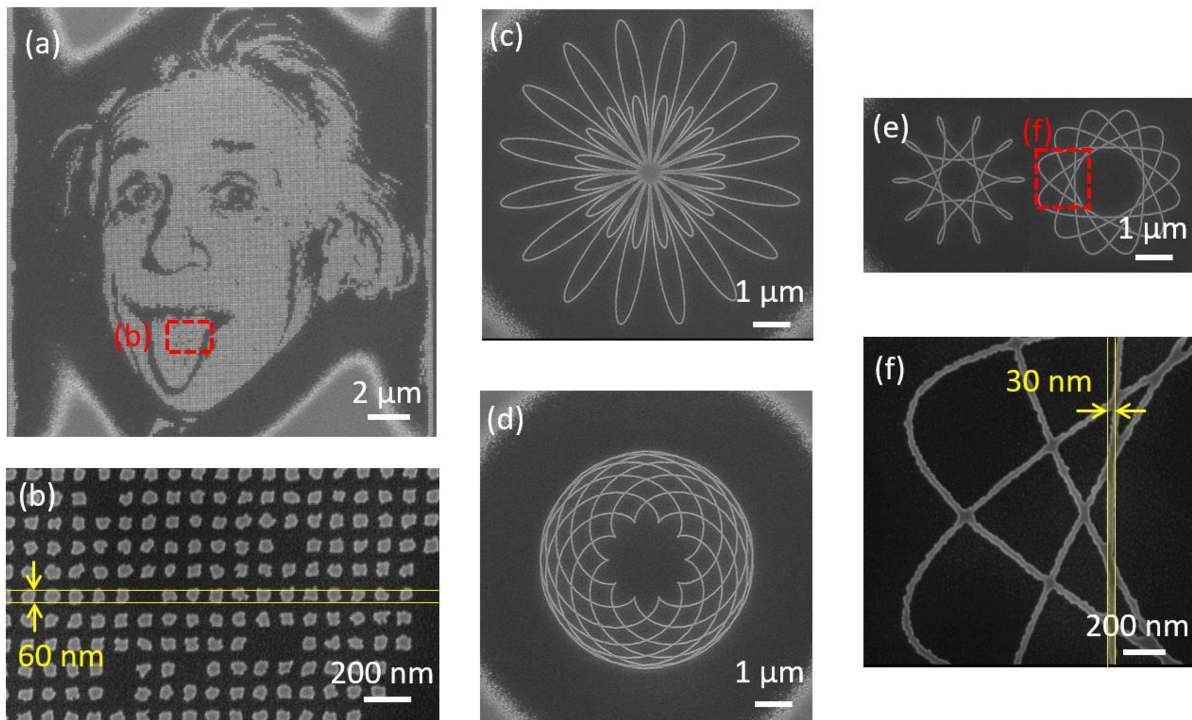

Figure 3.10 SEM image of various patterns on silicon substrate. (a) Einstein's picture exposed at 20 keV, 40,000 μC/cm², 60 nm pixel size; (b) zoom-in image of (a); (c) geometric pattern expressed by trigonometric function exposed at 20 keV, 200 nC/cm; (d) cycloid pattern exposed at 20 keV, 200 nC/cm; (e) trochoid patterns exposed at 20 keV, 200 nC/cm; and (f) zoom-in image of (e).

In order to achieve completely negative behavior, longer thermal development can be used, but the tradeoff against it is the decrease of the sensitivity. Figure 3.11 (a) and (b) show the SEM images of line arrays with thermal development of 360 °C for 4 minutes. After 4-minute thermal development, unexposed and lightly exposed PMMA was vaporized, so the result became completely negative behavior. Figure 3.11 (c) shows the result of AFM measurement of line arrays shown in Figure 3.11 (b).

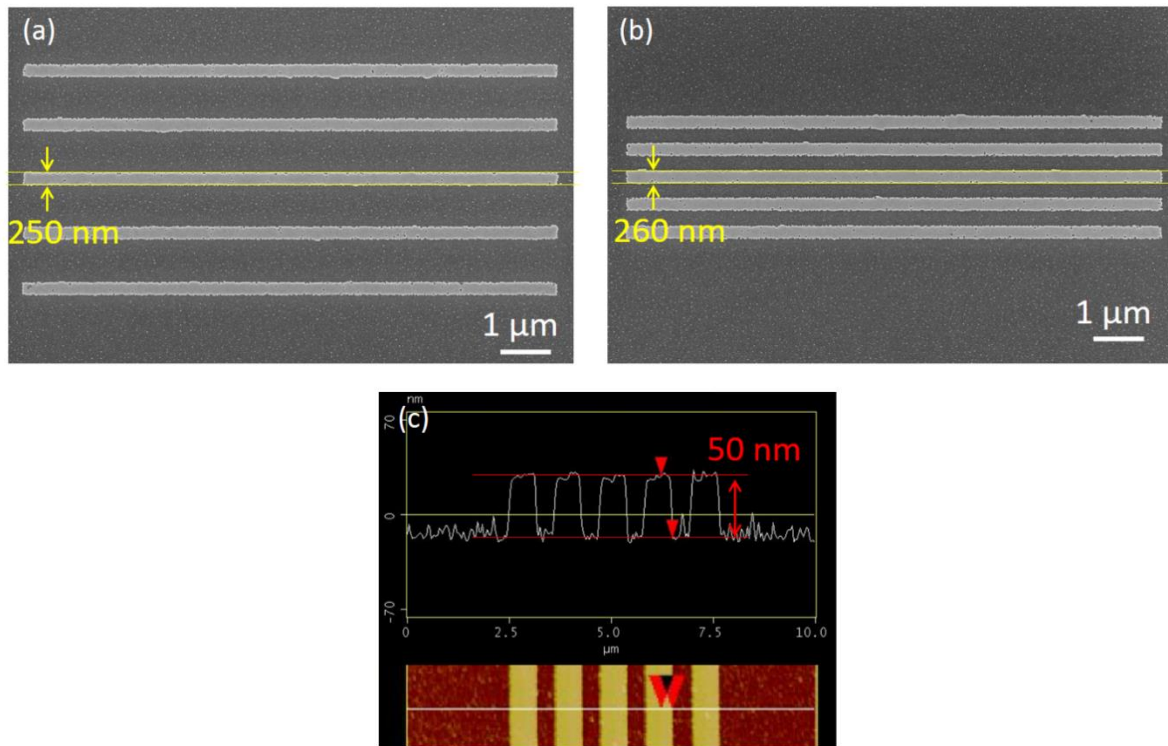

Figure 3.11 (a)(b) SEM images of line arrays etched into silicon. PMMA brush was exposed at 3 keV with area dose of 9,000 µC/cm², followed by thermal development of 360 °C for 4 minutes: (a) 1 µm period; and (b) 500 nm period. (c) AFM image of line arrays shown in (b).

3.3.6 Fabrication on AFM cantilever

Next, the fabrication on an AFM cantilever was performed. EBL was carried out at 20 keV, followed by thermal development at 365 °C for 1.5 minutes. Geometric and line array patterns were exposed at 400 nC/cm which resulted in 35 nm linewidth. As shown in Figure 3.12, even the patterns on non-flat surfaces of the cantilever were continuous and well-defined.

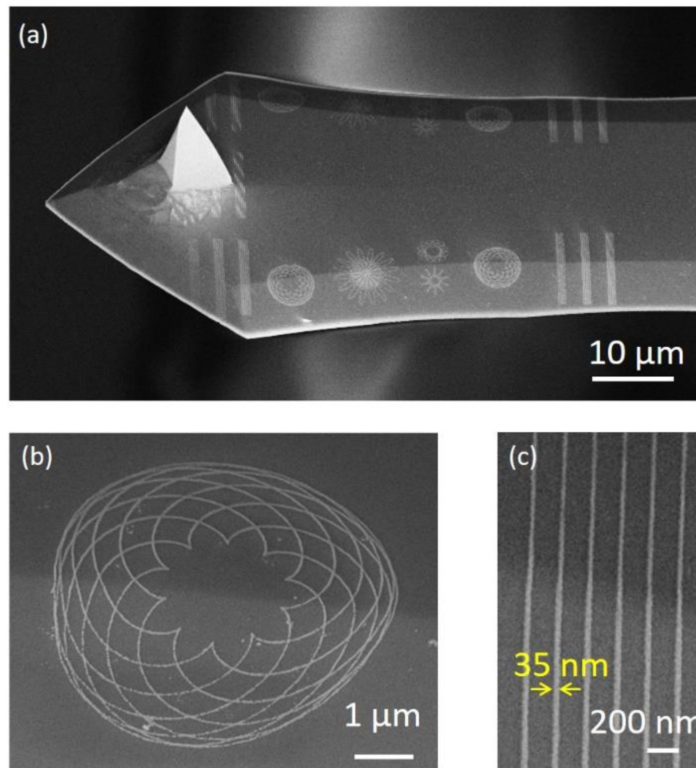

Figure 3.12 SEM images of line and geometrical patterns fabricated on non-flat region of an AFM cantilever: (a) top view; (b) zoom-in image of cycloid pattern, 20 keV, 400 nC/cm; (c) zoom-in image of line pattern, 20 keV, 400 nC/cm, period 200 nm.

3.4 Fabrication on fused silica substrate

So far, all the fabrications were performed on Si substrates. However, this process can be applied for any other substrates, such as fused silica or sapphire. Since the PMMA brush is bonded to the sacrificial metal layer, it can be grafted on any kinds of substrates. Here, we will demonstrate the fabrication on fused silica substrate using this process.

When fused silica substrate is used for electron beam lithography, charging effect can occur. Since fused silica is not conductive, electron accumulates on the substrate surface, which causes

electron beam deflection and pattern distortion. Charging effect can be reduced by coating conductive layer on the substrate, thus the sacrificial metal layer of our process can work to reduce charging effect. However, the oxidation of metal layer can be a problem. If the metal layer is too thin, all the layer is oxidized during the deposition and the metal layer cannot help reducing charging effect. The thickness of the metal layer depends on various factors, such as the deposition techniques, the kind of metal, and the base pressure during the deposition. In the case of thermal evaporated metal film, it was shown that metal oxide layer for Al, Cr, and Cu is less than 1 nm[36].

The process to fabricate nanoscale patterns on fused silica substrates is almost the same as that of Si substrates. PMMA brush was formed on fused silica substrate coated with 8 nm Cr layer. Cr deposition was performed by e-beam evaporation with the base pressure 4×10^{-6} Torr. Then, EBL was carried out at 3 keV. Because of 8 nm Cr layer, no charging effect was seen during the EBL. Then, PMMA brush was developed thermally at 360 °C for 1 minute. Cr wet etch was performed by Cr etchant (mixture of acetic acid (CH_3COOH), and ceric ammonium nitrate $(NH_4)_2[Ce(NO_3)_6]$) at room temperature for 2 seconds. Finally, fused silica substrate was etched by CF_4/O_2 RIE for 1 minute (20 sccm CF_4, 4 sccm O_2, 10 mTorr pressure, 50 W RF power)).

Figure 3.13 shows the SEM image and AFM measurement result of the protruded line arrays etched into fused silica substrate. The patterns are not well defined, and further optimization of the process is needed.

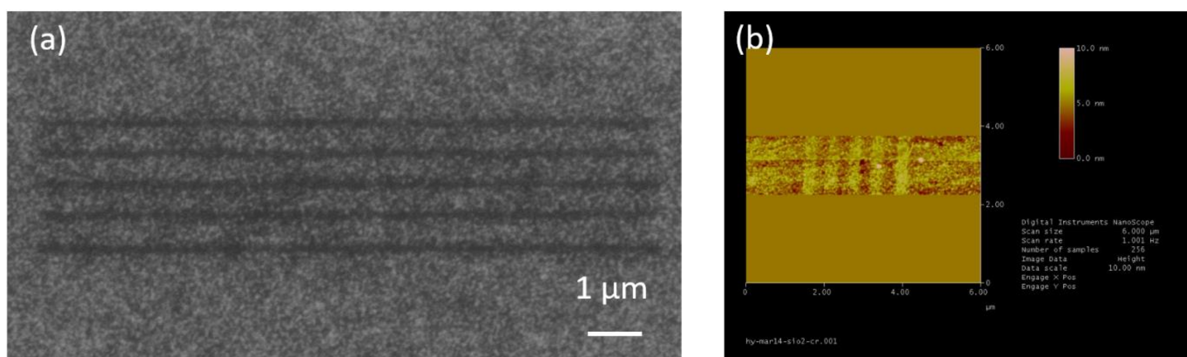

Figure 3.13 (a) SEM image of protruded line arrays fabricated on fused silica substrate, 3 keV, 5,000 µC/cm^2; and (b) the result of AFM measurement of the same patterns.

3.5 Summary and conclusions

We demonstrated that monolayer PMMA brush can be used as negative tone e-beam resist that is applicable for non-flat substrate. Although solvent such as acetone is used as a developer for bulk PMMA as a negative e-beam resist, solvent development did not work for PMMA brush. It was confirmed that PMMA brush exposed to electron beam failed to protect the underneath Al layer from wet etch. Thus, it cannot be used as a wet etch mask for pattern transfer to the underneath sacrificial Al layer even though heavily exposed PMMA remained after development. We found that when the heavily exposed PMMA brush underwent thermal development, it recovered the resistance to wet etch. Therefore, pattern transfer to the sacrificial metal layer was achieved using thermally developed PMMA brush. We obtained several structures on silicon substrates by performing dry etch of silicon using the sacrificial metal layer as a mask. Also, we applied the same process on an AFM cantilever, and showed that the method is applicable to non-flat substrates.

Chapter 4

Grafted polystyrene mono-layer brush as positive and negative tone e-beam resist

[This work is published in Langmuir[37].]

4.1 Introduction

Similar to PMMA, polystyrene (PS) can also be grafted on a substrate. PS is known as negative tone e-beam resist which is a low-cost resist with very long shelf life[16,38]. PS is often developed by solvent, such as tetrahydrofuran, xylene, chlorobenzene, or cyclohexane, but it is known that it can also be thermally developed[39].

In this study, PS mono-layer brush is used as electron beam resist. Although solvents are used to develop thick PS, they cannot be used for grafted PS monolayer as a developer because of the strong bonding between PS and substrate. Instead, negative tone behavior was achieved when the PS mono-layer film was thermally developed. Also, positive behavior was unexpectedly obtained when PS was coated on sacrificial aluminum layer and developed by diluted HF that etches the Al layer.

4.2 Experimental

Figure 4.1 shows the schematic diagram of the fabrication process on substrates by using monolayer PS brush as both positive and negative e-beam resist. First, a sacrificial metal layer (8-10nm Al or Cr layer) for pattern transfer was coated on the substrate because monolayer of PS is too thin to transfer pattern directly into substrate similar to PMMA brush. Then, carboxyl terminated polystyrene PS-COOH (molecular weight Mn=13 kg/mol, Scientific Polymer

Products) dissolved in toluene with a concentration of 10 w/v% was spin-coated on substrate. The film was then baked at 160 °C for 24 hours. The –COOH group in PS-COOH reacts with the –OH group on the surface of the substrate with the release of water during the baking. The bulk of PS-COOH was then washed away by soaking the film in xylene (mixture of isomers) for 1 minute. Since the bottom layer of PS-COOH is bonded to the substrate strongly, a grafted monolayer of PS-COOH remains on the substrate even after the xylene wash. Then, e-beam lithography was performed with the electron energy of 5 keV by LEO 1530 field emission SEM (Carl Zeiss) integrated with the nanometer pattern generation system (JC Nabity Lithography Systems).

The tone of resist (positive or negative) depends on the development method. To use PS brush as negative tone resist, the resist was thermally developed on a hotplate at 300 °C for 1 minute. Since the exposed and thus cross-linked PS is more thermally stable than unexposed PS, only the unexposed PS is vaporized at this temperature. Then the aluminum layer underneath the PS layer was etched by diluted hydrofluoric acid ($HF:H_2O$=1:500 volume ratio) for 70 seconds. Finally, the pattern was transferred into substrate by CF_4/O_2 RIE (20 sccm CF_4, 4 sccm O_2, 10 mTorr pressure, 50 W RF power).

On the other hand, the positive tone was achieved by diluted HF development. After the electron beam exposure, the PS film was soaked in diluted HF ($HF:H_2O$=1:25 volume ratio). The Al layer underneath exposed PS was etched by HF and the exposed area of PS brush layer was thus lifted off, whereas the Al layer underneath unexposed PS remained. This implied that PS film exposed to electron beam loses its ability to protect the underneath Al layer against HF wet etch. Finally, the pattern was transferred into substrate in the same way as negative tone process.

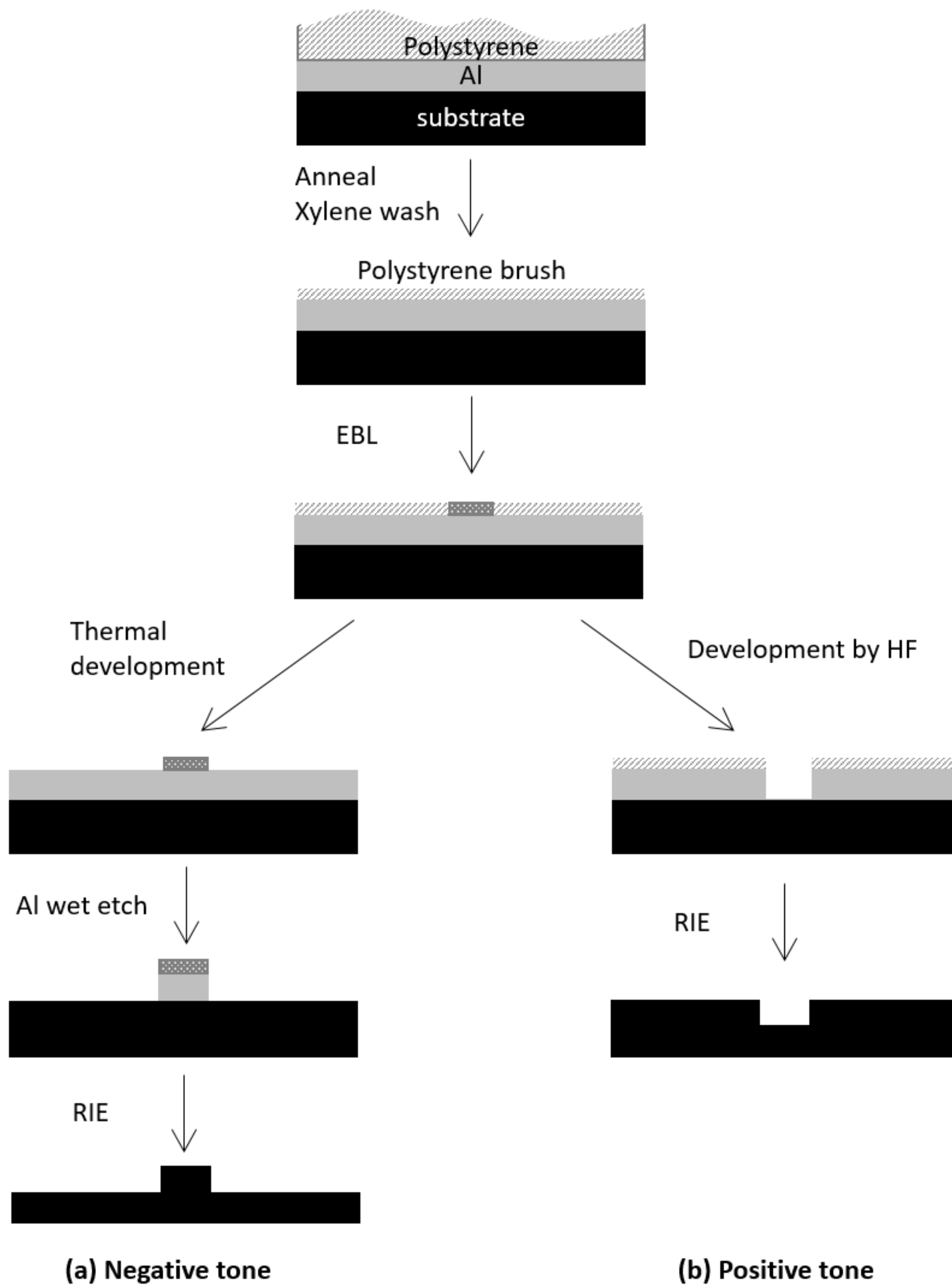

Figure 4.1 Process steps for patterning substrates using polystyrene mono-layer brush for both negative and positive e-beam resist.

4.3 Results and discussion

4.3.1 Packing density

The thickness of monolayer PS brush was measured 15 nm. Since the bulk density of polystyrene is 1.05 g/cm^3, the packing density is calculated as σ=0.72 chains/nm^2.

4.3.2 Negative tone results

As with thick PS film, monolayer PS brush can be used as negative e-beam resist. However, solvent development does not work for monolayer PS brush because solvent cannot cut the bonding between -COOH group in PS-COOH and -OH group on the surface of substrate. In order to check the solubility of PS brush in solvents, the monolayer PS brush film was soaked in tetrahydrofuran, a developer for thick PS film, for 20 minutes with ultrasonication. The film thickness did not change at all before and after soaking in tetrahydrofuran. It indicates that the bonding between PS brush and substrate is so strong that solvents cannot be a developer for PS brush.

Instead of solvent development, thermal development can be used. During the thermal treatment, PS undergoes random chain scissions and end-chain scission, which generates styrene monomer. Thus, regardless of the strong bonding between PS and substrates, degradation of PS film occurs. Since cross-linked PS has higher resistance toward thermal decomposition, only unexposed PS is vaporized and exposed PS remains if the proper temperature and time of thermal development is chosen. If the temperature is too high, both unexposed and exposed PS will be decomposed, and if the temperature is too low, even unexposed PS will not be decomposed completely.

Thermal development at several different conditions were examined to find the optimal thermal development conditions. エラー! 参照元が見つかりません。 shows the result of each condition. Some patterns were found on Si substrate after pattern transfer when the development temperature was between 250 °C and 325 °C, and the results were the most reproducible when it was developed at 300 °C for 1 minute.

Table 4.1 Thermal development condition and results. Circle symbols mean patterns are found on substrate after pattern transfer, and cross symbols mean there are no patterns on substrate after pattern transfer.

Temperature [°C]	Time [minutes]	Result
250	1	×
250	5	○
275	3	○
300	1	○
300	3	×
325	1	○
325	3	×
350	1	×

Figure 4.2 (a) and (b) show the SEM images of line arrays etched into silicon. EBL was carried out at 5 keV. Then, PS brush was developed thermally at 300 °C for 1 minute, followed by the aluminum wet etch by diluted HF ($HF:H_2O$=1:500 volume ratio) for 70 seconds. Finally, the patterns were transferred into Si substrate by CF_4/O_2 RIE for 2 minutes by using Al as a mask. Line arrays on silicon substrate with 110 nm width and 500 nm period, and 230 nm width and 1 µm period were obtained at 2.0 nC/cm and 3.8 nC/cm respectively. Figure 4.2 (c) shows the result of AFM measurement of line arrays shown in Figure 4.2 (b).

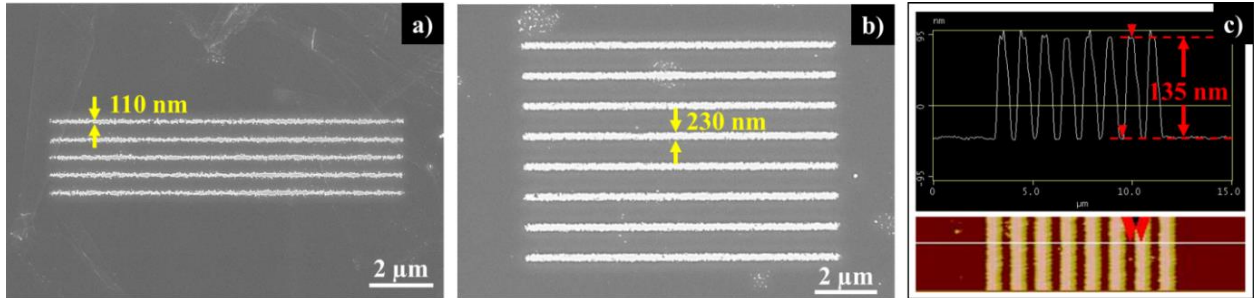

Figure 4.2 (a)(b) SEM images of protruded line arrays etched into silicon. PS brush was developed thermally at 300 °C for 1 minute: (a) 500 nm period, 2.2 nC/cm; and (b) 1 µm period 3.8 nC/cm. (c) AFM image of the line arrays shown in (b).

4.3.3 Positive tone results

Although bulk PS can be used only as a negative tone resist, grafted PS monolayer brush can work as positive tone resist when a sacrificial metal layer is used for pattern transfer. First, EBL was carried out at 5 keV. In order to achieve positive tone, the resist was developed by diluted HF ($HF:H_2O$=1:25 volume ratio) for 15 seconds. As with PMMA brush, PS brush exposed to electron beam lost the resistance to HF, and the Al layer underneath exposed PS was etched by HF. Therefore, the exposed area of PS brush was lifted off and only the unexposed area remained. Finally, the patterns on Al layer were transferred into Si substrate by 2-minute RIE. Figure 4.3 (a)-(c) show line arrays etched into silicon substrate with 40 nm width and 300 nm period, 25 nm width and 1 µm period, and 230 nm width and 500 nm period at 0.2 nC/cm, 0.2 nC/cm, and 3.8 nC/cm respectively. Figure 4.3 (d) shows the result of AFM measurement of the line arrays shown in Figure 4.3 (c). Since the AFM tip was not sharp enough, the tip did not reach the bottom of the trench. Therefore, the actual depth of the trenches was larger than the measured value by

AFM. The depth is expected to be the same as the protruded line arrays shown in Figure 4.2 (c) (which is 135 nm) because the same RIE recipe was used for both positive tone and negative tone results.

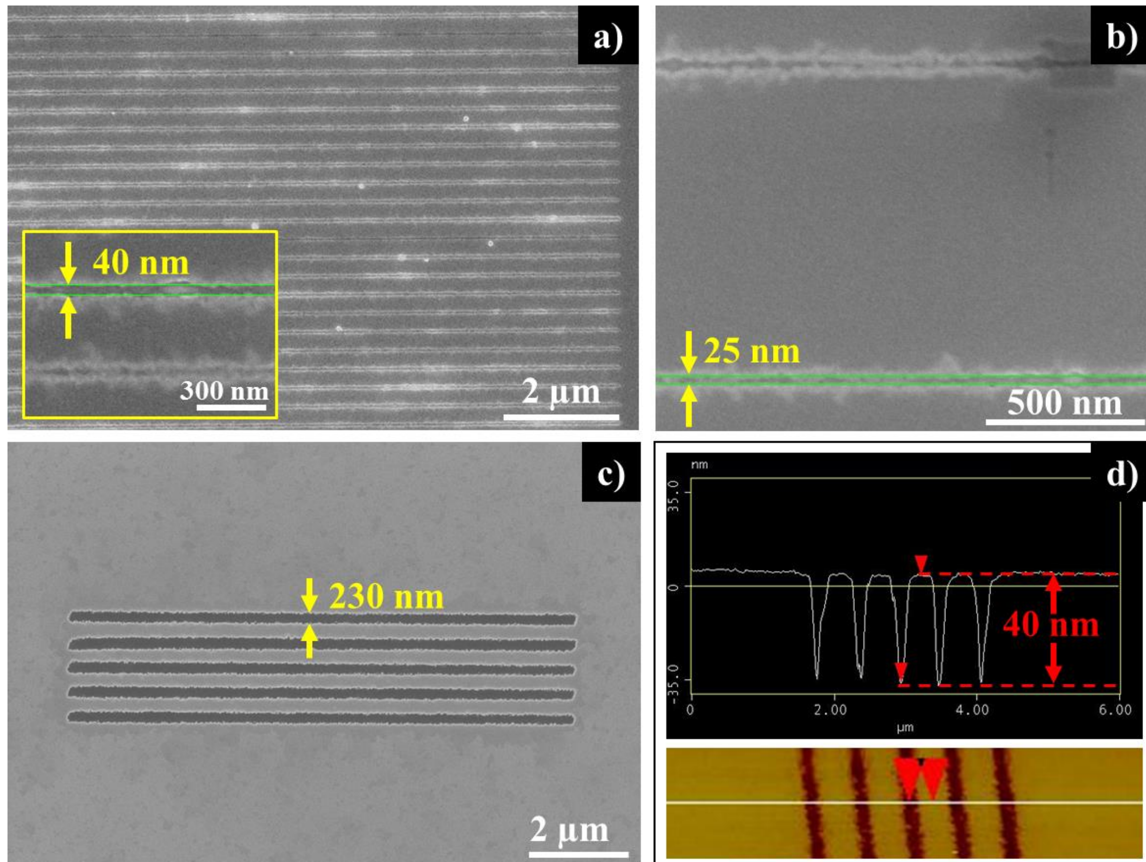

Figure 4.3 (a)-(c) SEM images of recessed line arrays etched into silicon. PS brush was developed by diluted HF for 15 seconds: (a) 300 nm period, 0.2 nC/cm; (b) 1 µm period 0.2 nC/cm; and (c) 500 nm period, 3.8 nC/cm. (d) AFM image of the line arrays shown in (c).

Although bulk PMMA is also used as positive and negative tone e-beam resist, the mechanism of PS brush and PMMA is different. When the PMMA film is exposed to electron beam at low dose, chain scissions occur and PMMA behaves as positive tone resist. However, when the PMMA film is exposed at high dose, cross-wlinking occurs and PMMA behaves as negative tone resist. Therefore, PMMA changes its behavior according to the amount of dose. On the other hand, PS brush changes its behavior according to the development method. The optimal electron dose also changes depending on the tone of the PS brush, but the dose does not play the critical role to change the tone of resist. For example, the doses for Figure 4.2 (b) and Figure 4.3 (c) are both 3.8 nC/cm, but the result shown in Figure 4.2 (b) behaves in negative tone, and the one shown in Figure 4.3 (c) behaves in positive tone. The results indicate that PS brush exposed to electron beam loses the resistance to HF, and it cannot protect underneath Al layer from being etched by HF.

4.4 Summary and conclusions

We demonstrated that monolayer PS brush can be grafted on substrates and used as both negative and positive e-beam resist. The tone of PS brush changed depending on development method. Bulk PS film is known as negative e-beam resist when it is developed by solvents, but solvents cannot be used for monolayer PS brush. Since the monolayer PS brush is strongly connected to the substrate, it is not dissolved into solvents. Instead of solvents, thermal development was used to achieve negative tone behavior. Exposed PS is cross-linked, and has higher thermal stability. Therefore, only unexposed PS is vaporized at proper temperature, and the PS brush works as negative tone e-beam resist.

Positive tone behavior was achieved when the PS brush was developed by diluted HF solution. PS brush exposed to electron beam loses the resistance to the HF, thus HF can etch the Al layer underneath the exposed PS brush directly.

We obtained well-defined structures on silicon substrates by performing dry etch of silicon using the sacrificial metal layer as a mask. The process can be applied to irregular substrates, which has various promising applications such as nanofabrication on AFM tips or fiber facets. It can provide a simple way to fabricate both recessed and protruded structures on those unconventional surfaces.

Chapter 5

Mixture of polystyrene and PDMS with high dry etch resistance as negative tone e-beam resist for potential HSQ replacement

This chapter is not related to the previous chapters and starts a new topic about a novel e-beam resist that has high dry etch resistance.

5.1 Introduction

Electron beam lithography (EBL) is one of the most popular nanolithography techniques for research and prototyping purposes. Typically, patterns made on electron beam resist are transferred into the substrate by direct dry etch using the resist as a mask or by lift-off process. Therefore, high resistance to dry etch is one of the important characteristics of electron beam resist. If the dry etch resistance of a resist is high, high aspect ratio patterns can be fabricated by direct dry etch method. Also, resist with high resistance to dry etch can be used for a negative tone lift-off process to make an undercut structure[40], which is important for a clean lift-off process.

Recently, HSQ has been vigorously studied as negative tone e-beam resist with high resolution and high resistance to dry etch. The resolution of HSQ is similar to that of the most popular positive resist, PMMA. 9-nm pitch nested-L structures were demonstrated by using 10-nm-thick HSQ[13]. Since HSQ is a silicon dioxide based inorganic material, it has higher dry etch resistance than ordinary polymer resists, such as PMMA or polystyrene. However, HSQ has several drawbacks: HSQ is very expensive, the shelf life is very short, and all the processes need to be done quickly to prevent the deterioration of the resist film by absorbing contaminants from

atmosphere[14,15]. Therefore, there is still a huge demand for cheap and easy-to-use resist with high dry etch resistance.

PDMS is a Si-based organic polymer, which is widely used as an elastic stamp material in soft lithography[41]. PDMS exists in the liquid phase at room temperature, and it is solidified when cross-linking occurs. A widely used method to achieve cross-linking is using catalysts[42], but it has been shown that electron beam or proton beam irradiation can also cause cross-linking to PDMS[43,44]. Since PDMS contains Si, it shows higher resistance against oxygen plasma etching compared to other organic polymers such as polystyrene[45].

In this work, we investigated the performance of polystyrene (PS) containing PDMS as a negative tone e-beam resist. PS is known as a negative tone e-beam resist that provides high resolution when low molecular weight PS is used, and high sensitivity when high molecular weight PS is used[16,38]. Also, the cost of PS is much lower than that of HSQ, and the shelf time is virtually unlimited. Since PDMS contains Si, the mixture of PS and PDMS is a good candidate for a high resolution or high sensitivity negative tone e-beam resist with high dry etch resistance. We showed that by adding PDMS into PS, the dry etch resistance against O_2 and SF_6/C_4F_8 RIE became much higher than that of pure PS, whereas the sensitivity and contrast of the resists remained nearly the same.

5.2 Experimental

Polystyrene (Mw=350 kg/mol, Mn=170 kg/mol, Sigma-Aldrich Co. LLC) and PDMS (Mw=6 kg/mol, Scientific Polymer Products, Inc) were dissolved in xylene or toluene together. The weight ratios of PS and PDMS were 5:2, 5:1, 10:1, 25:1 and 50:1. Then, the mixture of PS and PDMS were spin-coated on Si substrate on which PMMA brush was grafted in advance as an adhesion layer[46]. The film was then baked at 110 °C for 5 minutes.

Next, electron beam lithography was performed on the PS-PDMS film at 10 keV or 20 keV using LEO 1530 field emission SEM (Carl Zeiss) integrated with the nanometer pattern generation system (JC Nabity Lithography Systems). The film was then developed by xylene (mixture of isomers) for 30 seconds and rinsed by IPA.

The resistance to dry etch with O_2 or SF_6/C_4F_8 gases was tested by Oxford Instruments ICP380 dry etching system and Trion Technology Phantom II RIE system for the PS-PDMS film before and after e-beam exposure..

5.3 Results and discussions

5.3.1 Sensitivity and contrast

We first measured the contrast curves of pure PS and PS-PDMS mixtures. We exposed arrays of 4 μm squares on pure PS and PS-PDMS mixtures. Figure 5.1 (a) shows the contrast curves of pure PS and PS-PDMS (ratio 10:1) exposed at 20 keV. The contrast and sensitivity for PS and PS-PDMS were 2.1, 74 $\mu C/cm^2$, and 1.8, 70 $\mu C/cm^2$, respectively. Therefore, there was no drastic change in contrast and sensitivity between pure PS and PS-PDMS (ratio 10:1). The resist sensitivity was nearly 4 times higher than that of HSQ[47] exposed at the same electron energy, but the contrast was lower. Higher contrast can be attained by using lower molecular weight PS.

Figure 5.1 (b) shows the contrast curves of PS-PDMS with various ratios from 50:1 to 5:2 exposed at 10 keV. Even at the highest concentration of PDMS (PS:PDMS ratio 5:2), no major change in sensitivity and contrast was seen.

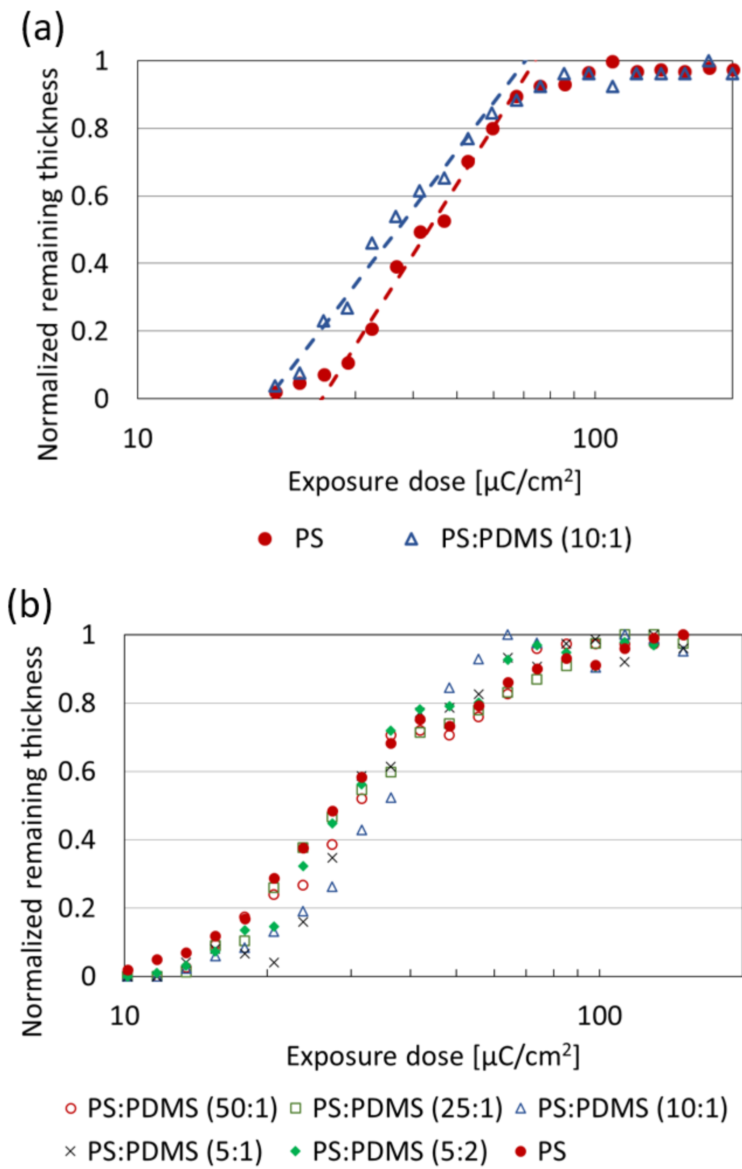

Figure 5.1 Contrast curves of pure PS and the mixture of PS and PDMS exposed at: (a) 20 keV; and (b) 10 keV.

5.3.2 Dry etch resistance

Then, dry etch resistance of PS-PDMS was examined. First, the etching rate by O_2 RIE (20 mTorr, O_2 20 sccm, RF power 20 W) of pure PS and the mixture of PS-PDMS (ratio 10:1) without e-beam

exposure was measured. Figure 5.2 shows the remaining resist thickness of the films after O_2 RIE. The etching rate of pure PS was 120 nm/minute, but the thickness change of PS-PDMS film was negligible even after 20-minute RIE. Figure 5.3 shows the AFM image of PS-PDMS film after 10-minute O_2 RIE. The film had a smooth surface even after O_2 RIE.

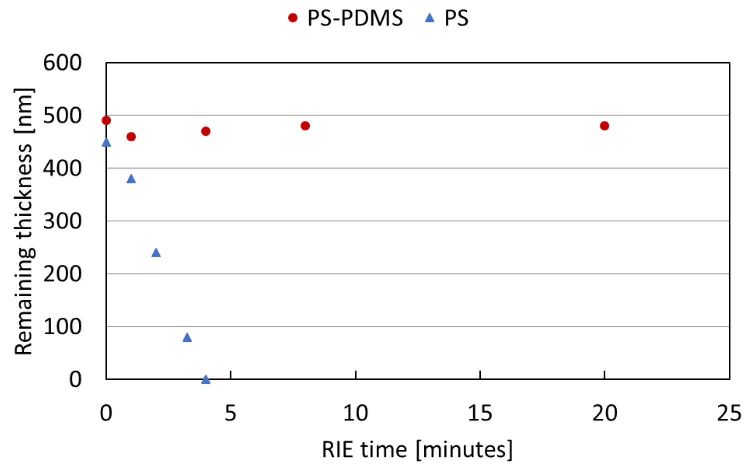

Figure 5.2 Remaining resist thickness after O_2 RIE (pure PS and PS-PDMS, ratio 10:1).

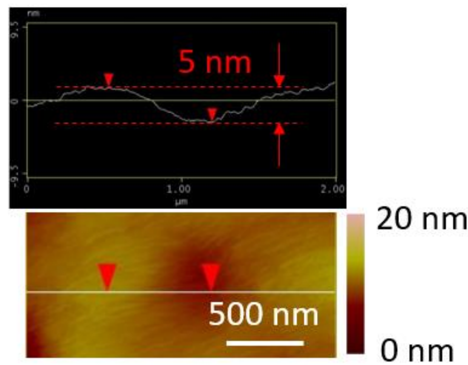

Figure 5.3 AFM image of 500-nm-thick PS-PDMS (ratio 10:1) film after 10-minute O_2 RIE.

Next, the effect of O_2 RIE after e-beam exposure and development was measured. 80-nm-thick PS-PDMS (ratio 50:1, 25:1, 10:1, 5:1, and 5:2) films were prepared on Si substrate with PMMA brush, and 4 μm square patterns on the films were exposed to electron beam at 10 keV with dose from 42 to 150 μC/cm^2, and then developed by xylene. The samples were then etched by O_2 RIE (20 mTorr, O_2 20 sccm, RF power 20 W). After 90-second O_2 RIE, all patterns on low PDMS concentration PS-PDMS (ratio 50:1 and 25:1) were confirmed to be etched away, but the patterns on higher PDMS concentration PS-PDMS (ratio 10:1, 5:1, and 5:2) still remained even after 210-second RIE.

Figure 5.4 shows the SEM images of the square patterns on PS-PDMS (ratio 10:1, 5:1 and 5:2) after 210-second O_2 RIE. As shown in Figure 5.4 (a1)-(a4), there were small holes on PS-PDMS (ratio 10:1). The number of holes decreased when the exposure dose is increased, but even the pattern exposed at 150 μC/cm^2 had several holes. A possible explanation is that there is some degree of phase separation between PS and PDMS at this concentration, and that at low dose exposure, only PS gets cross-linked and PDMS does not. Therefore, the uncross-linked part is removed during the development, which makes holes on the pattern. These holes were hardly seen on PS-PDMS with high PDMS concentration (ratio 5:2) as shown in Figure 5.4 (c1)-(c4), which indicates that the phase separation presumably does not exist at this concentration.

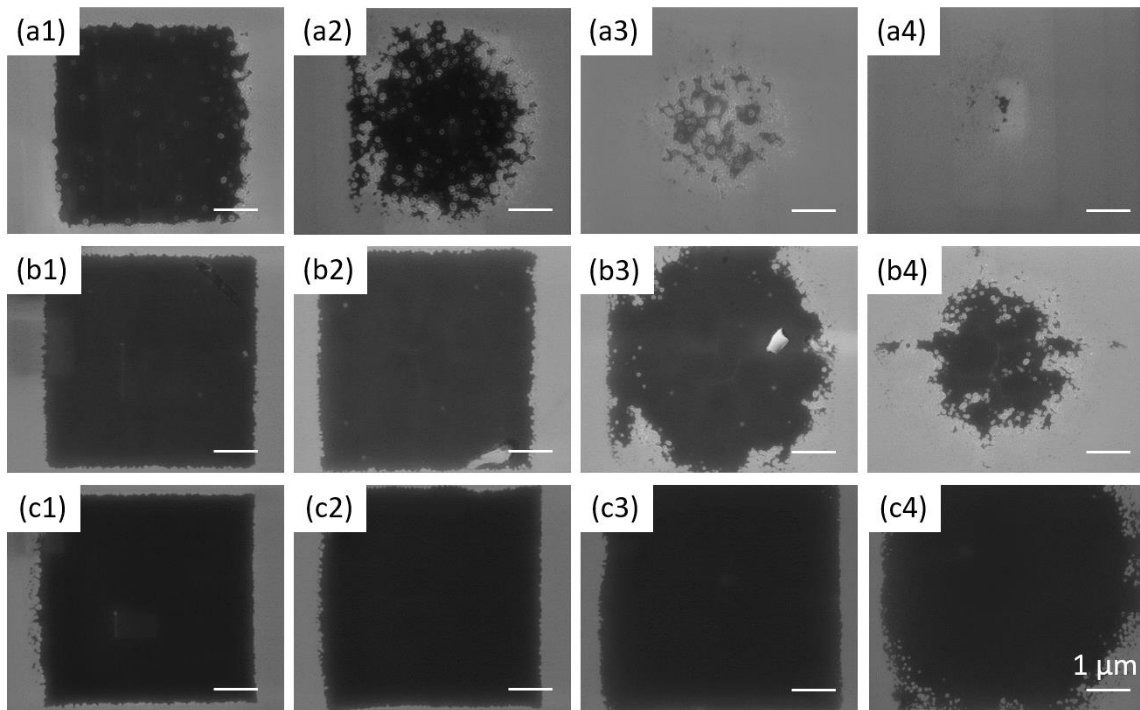

Figure 5.4 SEM images of PS-PDMS after e-beam exposure and 210-second O_2 RIE. The ratio of PS:PDMS is: (a1)-(a4) 10:1; (b1)-(b4) 5:1; and (c1)-(c4) 5:2. The exposure dose is: (a1)(b1)(c1) 150 μC/cm^2; (a2)(b2)(c2) 98 μC/cm^2; (a3)(b3)(c3) 64 μC/cm^2; and (a4)(b4)(c4) 42 μC/cm^2.

Next, the effect of dry etch for Si etching using non-switching deep Si etch process with SF_6 and C_4F_8 gases (20 sccm SF_6 and 40 sccm C_4F_8, 10 mTorr, 1200 W ICP power, and 20 W RF power, etching rate for Si: 380 nm/minute) was examined. Figure 5.5 shows the etching rate of pure PS and PS-PDMS film without e-beam exposure. The etching resistance of PS-PDMS (ratio 5:1 and 5:2) was approximately 2 times higher than that of pure PS.

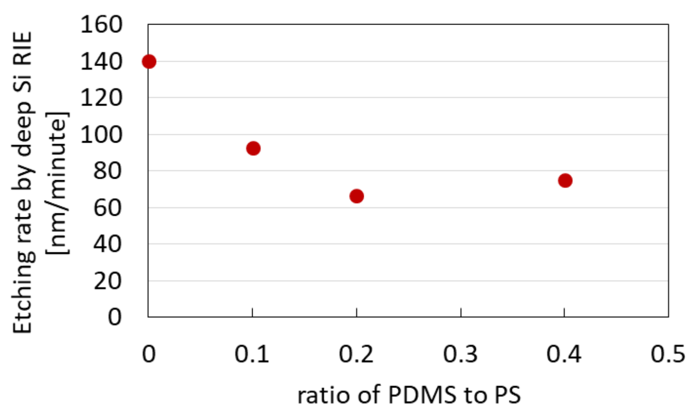

Figure 5.5 Etching rate of pure PS and PS-PDMS by deep Si RIE with SF_6 and C_4F_8 gases.

5.3.3 Line array patterns on Si wafer

Figure 5.6 shows the SEM images of line arrays on PS-PDMS (ratio 10:1). 200-nm-wide and 1-μm pitch line patterns were made on 250-nm-thick PS-PDMS film. The film was exposed at 20 keV, 200 $\mu C/cm^2$ and developed by xylene for 30 seconds. The line patterns were continuous after development. Then 150-second O_2 RIE (20 mTorr, O_2 20 sccm, RF power 20 W) was performed. After O_2 RIE, a portion of the lines was etched away and the patterns became discontinuous as shown in Figure 5.6 (b) and (c). This implies that there is some degree of phase separation as expected from the results of the previous subsection.

Figure 5.7 shows the SEM images of line arrays made on 80-nm-thick PS-PDMS (ratio 5:2) exposed at 10 keV, 100 $\mu C/cm^2$, followed by 210-second O_2 RIE. Unlike the line arrays on PS-PDMS (ratio 10:1), the lines were continuous even after O_2 RIE and the edge of the structures were well-defined, which indicates that there is no phase separation at this concentration. Corrugated structures were presumably caused by the capillary force during the development.

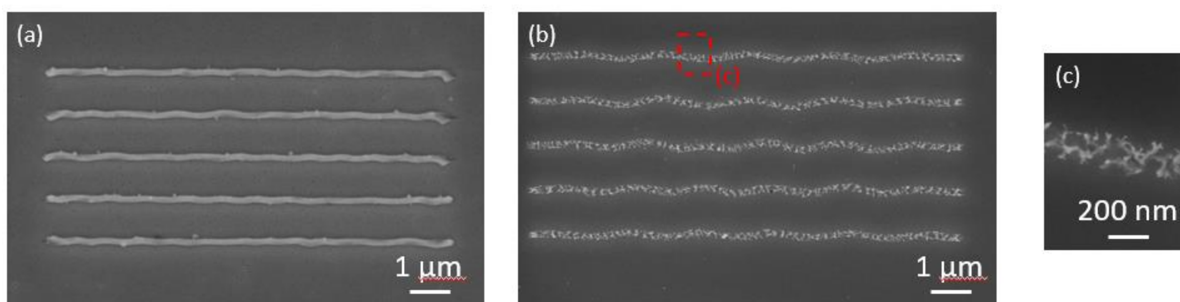

Figure 5.6 SEM images of line arrays on 250-nm-thick PS-PDMS (ratio 10:1): (a) Line arrays with 200 nm width, 1µm pitch, exposed at 20 keV, 200 µC/cm^2; (b) line arrays shown in (a) after 150-second O_2 RIE; and (c) zoom in image of (b).

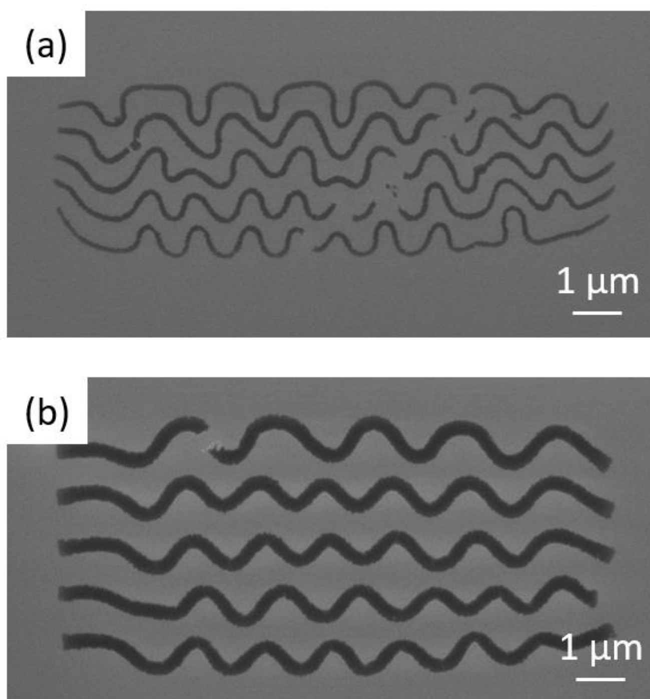

Figure 5.7 SEM images of line arrays on 80-nm-thick PS-PDMS (ratio 5:2) after 210-second O_2 RIE, exposed at 10 keV, 100 µC/cm^2: (a) 100 nm width; and (b) 250 nm width. The wavy resist structure is caused by capillary force.

5.4 Summary and conclusions

It was shown that the dry etch resistance against O_2 or SF_6/C_4F_8 RIE of PS-PDMS film was higher than that of pure PS, whereas the contrast and sensitivity remained nearly the same. Therefore, PS-PDMS can be used as a low-cost replacement of HSQ when a negative tone e-beam resist with high dry etch resistance is required. The sensitivity of PS-PDMS was nearly 4 times higher than HSQ, but with lower contrast. Since the sensitivity and contrast depend on the molecular weight of PS, high resolution PS-PDMS resist can be attained by using low molecular weight PS at the cost of sensitivity.

Some degree of phase separation between PS and PDMS was seen after O_2 RIE for 10:1 ratio PS-PDMS. However, the phase separation was not seen for 5:1 ratio and 5:2 ratio PS-PDMS. Line array patterns were fabricated on 5:2 ratio PS-PDMS, and the patterns remained well-defined even after 210-second O_2 RIE.

Chapter 6

Conclusion

We studied the characteristics of monolayer polymer brush as electron beam resist. It was shown that grafted PMMA brush works as negative tone e-beam resist when it is developed thermally. When the PMMA brush was developed at 360 °C for 1 minute, only moderately exposed PMMA decomposed and both unexposed and heavily exposed PMMA remained. When it was developed at 360 °C for 4 minutes, both unexposed and lightly exposed PMMA decomposed and only heavily exposed PMMA remained. However, the sensitivity became lower when the development time was longer.

The line patterns as thin as 14 nm width for 100 nm period and 20 nm width for 60 nm period were fabricated on a flat substrate by using PMMA brush as negative tone resist. Also, nanofabrication on AFM cantilevers was demonstrated. One drawback of PMMA brush as negative e-beam resist is its extremely low sensitivity. The dose required for negative tone PMMA was about 1000 times higher than that of positive tone PMMA.

It was shown that grafted PS brush also works as electron beam resist. Although bulk PS is only used as negative tone resist, PS brush can be used as both positive and negative resist. In order to achieve negative tone, PS brush needs to be developed thermally because solvents do not dissolve PS brush that is strongly connected to substrates. It was found that thermal development of 300 °C for 1 minute is the optimal condition to achieve negative tone behavior. In order to achieve positive tone, PS brush on sacrificial aluminum layer was etched by diluted HF. The Al layer underneath exposed PS layer was etched away by diluted HF, whereas Al layer beneath unexposed PS layer remained.

Both PMMA and PS monolayer brush can be applied for non-flat, irregular surfaces such as AFM tips, AFM cantilevers, or optical fiber facets. The process can provide a simple way to pattern on such unconventional substrates.

Also, the mixture of PS and PDMS was examined as novel e-beam resist material with high dry etch resistance. The sensitivity and contrast of PS-PDMS were the almost the same as those of pure PS when the ratio of PDMS to PS was as high as 40%, but the etching resistance against O_2 or SF_6/C_4F_8 RIE of PS-PDMS film was much higher than that of pure PS. Therefore, PS-PDMS can be a candidate for a low-cost replacement of HSQ resist when negative tone e-beam resist with high dry etch resistance is required.

The advantages and disadvantages of each resist are summarized in Table 6.1. The main advantages of PMMA brush and PS brush is that they are applicable to non-flat, irregular surfaces. As negative tone resist, PMMA brush has higher resolution than PS brush, but the sensitivity is lower. Both resists suffer from the line edge roughness because of the lateral etching of the intermediate Al mask layer. In order to avoid the lateral etching, thinner Al layer can be used to make wet etching time shorter. Also, Al layer can be etched by dry etch instead of wet etch for future work.

The main advantage of PS-PDMS mixture is that it is a low-cost negative tone resist with high dry etch resistance. It can be a replacement of HSQ when negative tone resist with high dry etch resistance is required. When 350 kg/mol PS is used, the sensitivity is 4 times higher than that of HSQ. In order to improve the resolution, low molecular weight PS can be used at the cost of sensitivity for future work.

Table 6.1 Advantages and disadvantages of each e-beam resist.

	Advantages	Disadvantages
PMMA brush (negative)	· It is applicable to non-flat, irregular surfaces. · It is low-cost resist with long shelf time. · The resolution is high.	· Intermediate metal layer is required for pattern transfer. · The line edge of the patterns is rough. · Wet etch process and thermal development process is not well controllable. · The sensitivity is very low.
PS brush (negative)	· It is applicable to non-flat, irregular surfaces. · It is low-cost resist with long shelf time. · Sensitivity is higher than PMMA brush. · Dry etch resistance is higher than PMMA brush, thus pattern transfer to intermediate metal layer using dry etch might be possible.	· Intermediate metal layer is required for pattern transfer. · The line edge of the patterns is rough. · Wet etch process and thermal development process is not well controllable.
PS brush (positive)	· It is applicable to non-flat, irregular surfaces. · It is low-cost resist with long shelf time.	· Intermediate metal layer is required for pattern transfer. · The line edge of the patterns is rough. · Wet etch process is not well controllable.
PS-PDMS	· It has higher resistance against dry etch than pure PS. · Both PS and PDMS are low-cost, and have long shelf time. · The sensitivity is 4 times higher than that of HSQ when 350 kg/mol PS is used. · Resolution and sensitivity are controllable by changing the molecular weight of PS.	· Phase separation can occur depending on the ratio of the mixture.

References

1. Tseng, A. A. *Nanofabrication: Fundamentals and Applications*. (World Scientific Publishing Co. Pte. Ltd., 2008).

2. Dashen, R. F. Theory of electron backscattering. *Phys. Rev.* **134,** A1025–A1032 (1964).

3. Kyser, D. F. & Viswanathan, N. S. Monte Carlo simulation of spatially distributed beams in electron-beam lithography. *J. Vac. Sci. Technol.* **12,** 1305–1308 (1975).

4. Chang, T. H. P. Proximity effect in electron-beam lithography. *J. Vac. Sci. Technol.* **12,** 1271–1275 (1975).

5. Soe, E., Choi, B. K. & Kim, O. Determination of proximity effect parameters and the shape bias parameter in electron beam lithography. *Microelectron. Eng.* **53,** 305–308 (2000).

6. Owen, G. Methods for proximity effect correction in electron lithography. *J. Vac. Sci. Technol. B* **8,** 1889–1892 (1990).

7. Aya, S., Kise, K., Yabe, H. & Marumoto, K. Validity of double and triple Gaussian functions for proximity effect correction in X-ray mask writing. *Jpn. J. Appl. Phys.* **35,** 1929–1936 (1996).

8. McCord, M. A. & Rooks, M. J. *Handbook of Micromachining and Microfabrication. Volume 1: Microlithography*. (SPIE Press Book, 1997).

9. Fischbein, M. D. & Drndić, M. Nanogaps by direct lithography for high-resolution imaging and electronic characterization of nanostructures. *Appl. Phys. Lett.* **88,** 63116 (2006).

10. Haller, I., Hatzakis, M. & Srinivasan, R. High-resolution Positive Resists for Electron-beam Exposure. *IBM J. Res. Dev.* **12,** 251–256 (1968).

11. Koshelev, K. *et al.* Comparison between ZEP and PMMA resists for nanoscale electron beam lithography experimentally and by numerical modeling. *J. Vac. Sci. Technol. B* **29,** 06F306 (2011).

12. Frye, C. L. & Collins, W. T. The Oligomeric Silsesquioxanes, (HSiO3/2)n. *J. Am. Chem. Soc.* **92,** 5586–5588 (1970).

13. Yang, J. K. W. *et al.* Understanding of hydrogen silsesquioxane electron resist for sub-5-nm-half-pitch lithography. *J. Vac. Sci. Technol. B* **27,** 2622–2627 (2009).

14. Delft, F. C. M. J. M. Van. Delay-time and aging effects on contrast and sensitivity of hydrogen silsesquioxane. *J. Vac. Sci. Technol. B* **20,** 2932–2936 (2002).

15. Clark, N. *et al.* Time-dependent exposure dose of hydrogen silsesquioxane when used as a negative electron-beam resist. *J. Vac. Sci. Technol. B* **24,** 3073–3076 (2006).

16. Ma, S., Con, C., Yavuz, M. & Cui, B. Polystyrene negative resist for high-resolution electron beam lithography. *Nanoscale Res. Lett.* **6,** 446 (2011).

17. Yeo, B. S., Stadler, J., Schmid, T., Zenobi, R. & Zhang, W. Tip-enhanced Raman Spectroscopy – Its status, challenges and future directions. *Chem. Phys. Lett.* **472,** 1–13 (2009).

18. Consales, M. *et al.* Lab-on-fiber technology: Toward multifunctional optical nanoprobes. *ACS Nano* **6,** 3163–3170 (2012).

19. Han, A., Kuan, A., Golovchenko, J. & Branton, D. Nanopatterning on nonplanar and fragile substrates with ice resists. *Nano Lett.* **12,** 1018–1021 (2012).

20. King, G. M., Schürmann, G., Branton, D. & Golovchenko, J. A. Nanometer patterning with ice. *Nano Lett.* **5,** 1157–1160 (2005).

21. Zhang, J., Con, C. & Cui, B. Electron beam lithography on irregular surfaces using an evaporated resist. *ACS Nano* **8,** 3483–3489 (2014).

22. Con, C., Zhang, J. & Cui, B. Nanofabrication of high aspect ratio structures using an evaporated resist containing metal. *Nanotechnology* **25,** 175301 (2014).

23. Linden, J. *et al.* Spray coating of PMMA for pattern transfer via electron beam lithography on surfaces with high topography. *Microelectron. Eng.* **88,** 2030–2032 (2011).

24. Yamazaki, K. & Yamaguchi, H. Resist coating on vertical side faces using conventional spin coating for creating three-dimensional nanostructures in semiconductors. *Appl. Phys. Express* **3,** 106501 (2010).

25. Yamazaki, K. & Yamaguchi, H. Electron beam lithography on vertical side faces of micrometer-order Si block. *J. Vac. Sci. Technol. B* **30,** 41601 (2012).

26. Zhou, H. *et al.* Lithographically defined nano and micro sensors using 'float coating' of resist and electron beam lithography. *J. Vac. Sci. Technol. B* **18,** 3594–3599 (2000).

27. Glass, R. *et al.* Micro-nanostructured interfaces fabricated by the use of inorganic block copolymer micellar monolayers as negative resist for electron-beam lithography. *Adv. Funct. Mater.* **13,** 569–575 (2003).

28. Dey, R. K., Aydinoglu, F. & Cui, B. Electron Beam Lithography on Irregular Surface Using Grafted PMMA Monolayer as Resist. *Adv. Mater. Interfaces* **4,** 1600780 (2017).

29. Milner, S. T. Polymer Brushes. *Science* **251,** 905–914 (1991).

30. Kim, M., Schmitt, S. K., Choi, J. W., Krutty, J. D. & Gopalan, P. From self-assembled monolayers to coatings: Advances in the synthesis and nanobio applications of polymer brushes. *Polymers (Basel).* **7,** 1346–1378 (2015).

31. Hoole, A. C. F., Welland, M. E. & Broers, A. N. Negative PMMA as a high-resolution resist - the limits and possibilities. *Semicond. Sci. Technol.* **12,** 1166–1170 (1997).

32. Duan, H. *et al.* Sub-10-nm half-pitch electron-beam lithography by using poly(methyl methacrylate) as a negative resist. *J. Vac. Sci. Technol. B* **28,** C6C58-C6C62 (2010).

33. Beyler, C. L. & Hirschler, M. M. Thermal Decomposition of Polymers. *SPE Handb. Fire Prot. Eng.* 110–131 (2001). doi:10.1021/cm200949v

34. Lin, B. J. Deep uv lithography. *J. Vac. Sci. Technol.* **12,** 1317–1320 (1975).

35. Choi, J. O. Degradation of poly(methylmethacrylate) by deep ultraviolet, x-ray, electron beam, and proton beam irradiations. *J. Vac. Sci. Technol. B* **6,** 2286–2289 (1988).

36. Samantaray, C. B. & Hastings, J. T. The effect of thin metal overlayers on the electron beam exposure of polymethyl methacrylate. *J. Vac. Sci. Technol. B* **26,** 2300–2305 (2008).

37. Aydinoglu, F., Yamada, H., Dey, R. K. & Cui, B. Grafted Polystyrene Monolayer Brush as Both Negative and Positive Tone Electron Beam Resist. *Langmuir* **33,** 4981–4985 (2017).

38. Con, C. *et al.* High molecular weight polystyrene as very sensitive electron beam resist. *Microelectron. Eng.* **98,** 254–257 (2012).

39. Con, C., Abbas, A. S., Yavuz, M. & Cui, B. Dry thermal development of negative electron beam resist polystyrene. *Adv. nano Res.* **1,** 105–109 (2013).

40. Yang, H. *et al.* Electron beam lithography of HSQ/PMMA bilayer resists for negative tone lift-off process. *Microelectron. Eng.* **85,** 814–817 (2008).

41. Xia, Y. & Whitesides, G. M. Soft lithography. *Annu. Rev. Mater. Sci.* **28,** 153–184 (1998).

42. Baquey, G., Moine, L., Babot, O., Degueil, M. & Maillard, B. Model study of the crosslinking of polydimethylsiloxanes by peroxides. *Polymer (Guildf).* **46,** 6283–6292 (2005).

43. Bowen, J., Cheneler, D. & Robinson, A. P. G. Direct e-beam lithography of PDMS. *Microelectron. Eng.* **97,** 34–37 (2012).

44. Huszank, R., Rajta, I. & Cserháti, C. Proton beam lithography in negative tone liquid phase PDMS polymer resist. *Nucl. Instruments Methods Phys. Res. Sect. B* **348,** 213–217 (2015).

45. Babich, E., Paraszczak, J., Hatzakis, M., Shaw, J. & Grenon, B. J. A comparison of the electron beam sensitivities and relative oxygen plasma etch rates of various organosilicon polymers. *Microelectron. Eng.* **3,** 279–291 (1985).

46. Viscomi, F. N., Dey, R. K., Caputo, R. & Cui, B. Enhanced adhesion of electron beam resist by grafted monolayer poly(methylmethacrylate- co -methacrylic acid) brush. *J. Vac. Sci. Technol. B* **33,** 06FD06 (2015).

47. Yang, H. *et al.* Low-energy electron-beam lithography of hydrogen silsesquioxane. *Microelectron. Eng.* **83,** 788–791 (2006).